

We get technical

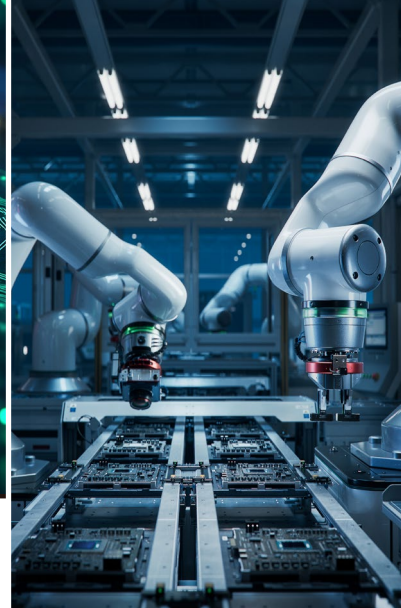
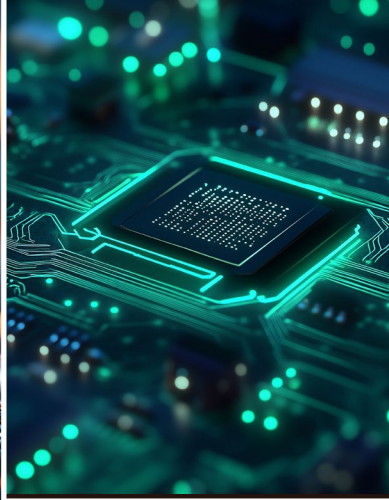
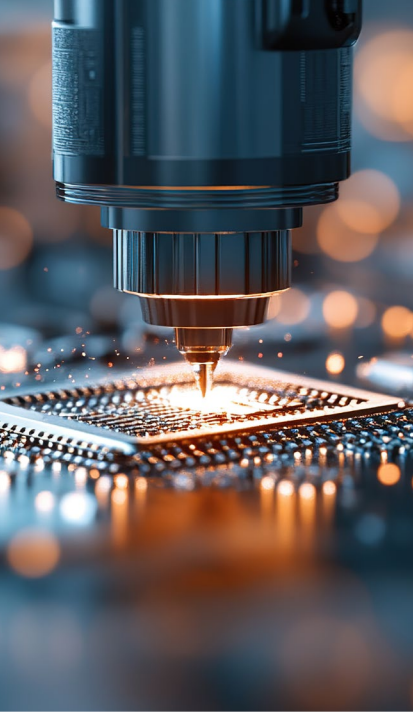
Advancing magnetic sensing

ADI's data acquisition solution shines in advanced lithography chip manufacturing

Arduino sample code for SPI absolute encoders

Accelerate your electronics projects





contents

- 4** Precision in a flash with direct time of flight sensing **amun OSRAM**
- 8** How low-power overmolded reed switches solve vexing position sensing challenges **Littelfuse®**
Expertise Applied | Answers Delivered
- 12** How A2L sensors make sure refrigerants don't blow(up)
- 16** Advancing magnetic sensing with Allegro MicroSystems' Tunnel Magnetoresistance (TMR) technology
- 22** **Special feature: retroelectro**
Experiments on the effect of a current of electricity on the magnetic needle
- 32** ADI's data acquisition solution shines in advanced lithography chip manufacturing
- 38** Take advantage of I3C for faster, simpler, and more flexible IC-to-IC communication
- 46** Arduino sample code for SPI absolute encoders
- 54** Learn the fundamentals of signal integrity
- 62** Accelerate your electronics projects with Scheme-it and DigiKey's extensive component catalog

Editor's note

Welcome to the DigiKey eMagazine Volume 19 – Sensors.

This edition will deep dive into the latest advancements in sensor technologies, data acquisition systems, and communication protocols, all of which are shaping the future of the electronics and semiconductor industries. As the pace of innovation accelerates, understanding these emerging technologies is crucial for both engineers and technologists looking to stay ahead.

In this issue, we explore the intricacies of Time-of-Flight Sensing, and Proximity and Limit Sensing, two essential technologies that enable precision in a wide array of applications from automotive to consumer electronics. We also take a closer look at A2L Sensors, exploring their capabilities and real-world applications, and uncover the potential of Tunnel Magnetoresistance (TMR) Technology, a breakthrough in sensor efficiency.

For those involved in chip manufacturing, our feature on Data Acquisition Solutions in Advanced Lithography provides insights into cutting-edge techniques driving semiconductor fabrication forward. Meanwhile, the I3C Communication Protocol article offers an in-depth look at how this technology is revolutionizing IC-to-IC communication, enabling faster and more flexible solutions.

We're also thrilled to include practical resources, such as Arduino Sample Code for SPI Absolute Encoders, making it easier than ever for hobbyists and professionals alike to integrate these technologies into their projects. And for those looking to expand their knowledge, our article on Signal Integrity Fundamentals will help sharpen your understanding of this vital aspect of modern electronics design.

Whether you are a seasoned engineer or a curious learner, this issue is packed with valuable insights and practical knowledge to enhance your understanding and keep you at the forefront of these dynamic fields.

Thank you for reading, and we hope you find inspiration and innovation on every page.

Precision in a flash with direct time of flight sensing

By Jeff Shepard

Contributed by DigiKey's North American Editors



A smartphone user frames a shot of their cat crouched in the hallway shadows. Pulses of light travel from the device, bounce off the cat, and return — allowing the phone's direct time-of-flight (dToF) sensor to precisely measure distance. The phone automatically sharpens its focus, producing a crisp, clear image. This seamless experience, taken for granted by millions of users, is the result of finely tuned optical sensing technology working behind the scenes.

But dToF isn't just advancing smartphone photography. This same technology is making its way into industrial automation and consumer electronics, where devices are increasingly relying on spatial awareness to trigger functions or adapt intelligently to user behavior. Whether it's a robot vacuum effortlessly dodging furniture and curious pets, or a facial recognition system that wakes up when someone approaches — dToF sensors are enabling intuitive interactions within a broad spectrum of environments.

In this article, we will explore the fundamentals of dToF sensing, and how the TMF8806 sensor from ams OSRAM is enhancing ranging solutions.

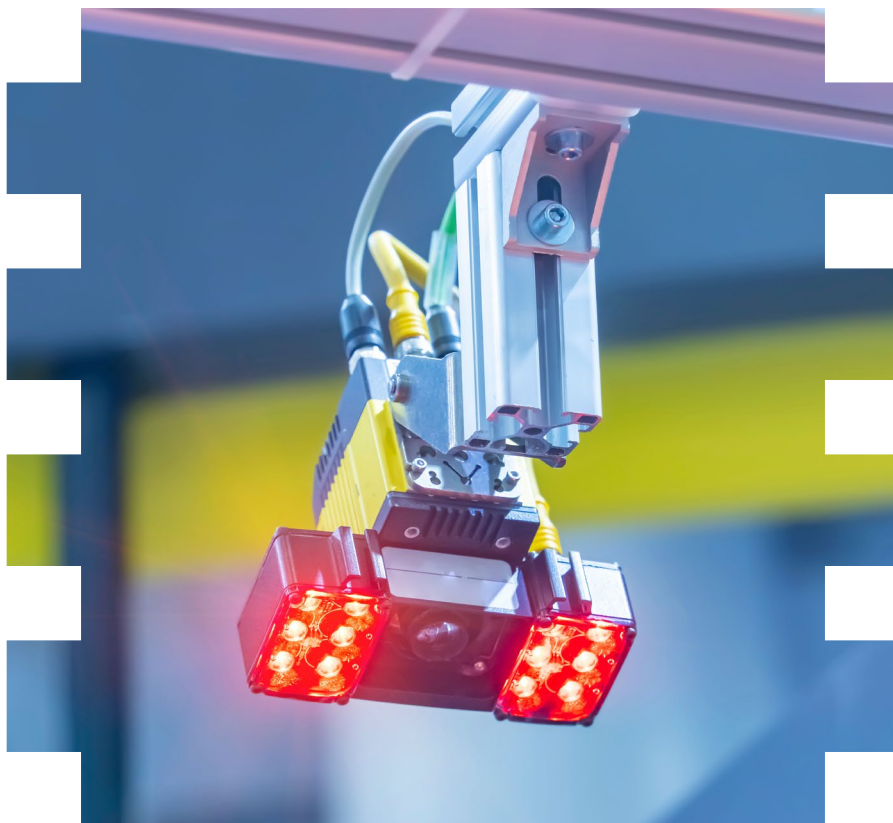
How dToF sensors work

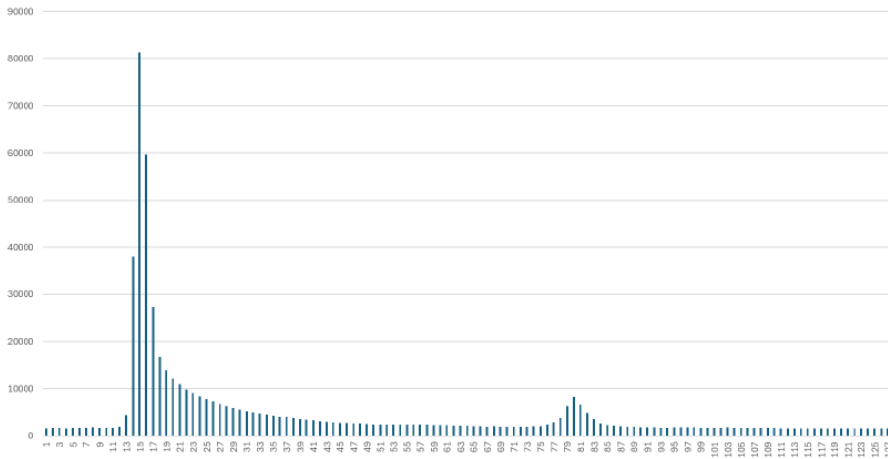
A dToF sensor operates by emitting an extremely short pulse of infrared light using a vertical cavity surface emitting laser (VCSEL). (By

extremely short, we're talking a few hundred picoseconds.) When this light hits an object and reflects back, the sensor detects it using an array of single photon avalanche diodes (SPADs), which are highly sensitive to even the faintest returning photons. The sensor's time-to-digital converter (TDC) acts as a stopwatch, measuring the time taken from pulse emission to the received signal. Since the speed of light is a known constant, the distance to the object can be calculated using the formula:

$$\text{Measured Distance} = \frac{\text{Photo Travel Time}}{2} \times \text{Speed of Light}$$

A single pulse isn't enough to ensure accuracy, so the sensor fires off hundreds of thousands of pulses per measurement cycle. The results are compiled into a histogram and processed by an embedded microcontroller, which determines the distance along with a confidence score based on the signal-to-noise ratio (SNR). This data is transmitted via a simple I²C interface.





A sample histogram demonstrating multiple pulses of light. (Image: ams OSRAM.)

While the sensor won't be fazed by a little dust or smudge on the cover glass, excessive buildup can degrade performance over time. Furthermore, the number of measurements taken per second varies by application. For instance, a video camera autofocus system may require 30 measurements per second, while presence detection in a smart appliance may need only a few per second. Higher measurement rates increase power consumption due to the higher number of VCSEL pulses.

Single-zone dToF sensors focus on detecting the closest object within a fixed field of view. Due to their compact nature, single-zone dToF sensors are generally well-suited to systems where space and power is limited.

Introducing the TMF8806 sensor

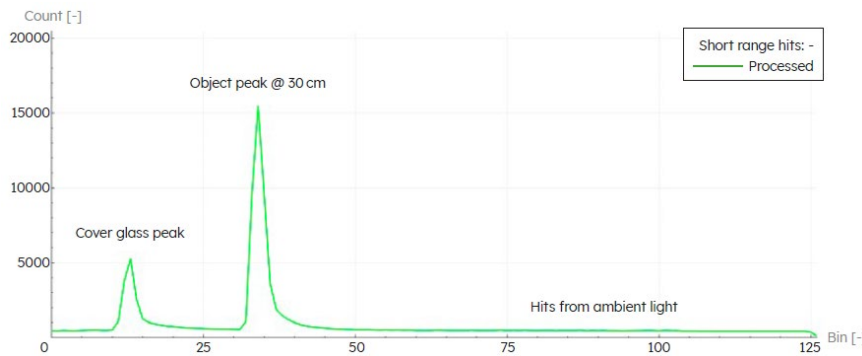
The [TMF8806](#) from ams OSRAM is a single-zone dToF sensor designed to detect objects from as close as 1 cm to as far as 10 m. Within its tiny footprint of just $2.2 \times 3.6 \times 1$ mm, the device includes a VCSEL emitter, SPAD array, TDC and on-chip histogram processing in one fully integrated module, making it easy to implement in various settings.

One of the key improvements in the TMF8806 is its expanded distance sensing capability. The sensor operates in standard 2.5-meter and 5-meter modes without requiring a firmware download, leading to faster startup and more power-efficient operation. A firmware update enables the extended 10-meter range for applications requiring longer-distance sensing.

Let's talk about the TMF8806's power efficiency in a little more detail.

The sensor can operate in ultra-low power modes, consuming as little as 14 μ A at a 0.5 Hz measurement rate. Even at 30 Hz, power consumption remains at just 27 mA. Because the TMF8806 features extremely fast startup – less than 5 ms – it allows users to switch the device off between measurements. Users can control the duty cycle from their host microcontrollers, which currently operate in sub-microamp modes. In other words, by using the microcontroller to wake up the sensor, take a measurement and go back to sleep, users can achieve highly efficient duty cycles and overall power consumption.

The TMF8806 also offers greater design flexibility. It supports multiple optical configurations, including a default mode optimized for minimal cover glass, a large air gap mode allowing up to 20 mm between the sensor and the outer surface, and a thick cover glass mode that supports protective layers up to 3.2 mm thick. This adaptability makes the sensor ideal for industrial applications, where thicker glass and greater mechanical tolerances are common. It is generally recommended to include an optical barrier or isolator between the cover glass and the sensor, as this helps to reduce production tolerances and improve performance.



*How the histogram distinguishes between detected objects and noise.
(Image: ams OSRAM.)*

The sensor further has the ability to support a lower interface voltage of 1.2-V I²C, in addition to the higher voltages that other ams OSRAM devices offer. This enables it to connect with a wide range of host processors, such as higher-integration processors that are becoming more widely used. The TMF8806's parts are rated for operation across a broad temperature range (-40 to 85°C), and support a voltage supply range of up to 3.5 V.

The TMF8806 also features improvements in electromagnetic compatibility (EMC), with the ability to enable spread spectrum modes for reducing electrical noise interference. Users can additionally set thresholds for lower and upper limits, where the sensor will only trigger an interrupt or report an object within a preset distance.

The TMF8806 operates with a 940-nm VCSEL, which includes built-in Class 1 eye safety circuitry. This system actively monitors the VCSEL and shuts down the driver if a fault is detected. The device also incorporates sunlight rejection filters to enhance outdoor performance. For applications requiring even stronger sunlight rejection, users can apply additional external filtering on the cover glass to further improve accuracy in bright environments.

At the core of the TMF8806 is a high-sensitivity SPAD detection system and a fast TDC architecture, capable of processing sub-nanosecond light pulses, as mentioned earlier. It has a high SNR and wide dynamic range. Its built-in crosstalk compensation minimizes false readings from cover glass reflections, and it can reject multipath interference. As a

result, the sensor achieves excellent resolution and maintains accurate distance measurements within $\pm 5\%$ in both dark and bright conditions.


Conclusion

The TMF8806 represents a step forward in dToF sensing. With built-in 2.5-meter and 5-meter modes that don't require a firmware download, it streamlines development for engineers looking to add precise ranging to their designs — whether for wake-on-approach interfaces, robotic navigation, or touchless interaction.

But the real beauty of the TMF8806 is how it is built to fit into the real world. Its ultra-low power operation makes it a natural choice for low-power systems, while its flexible optical configurations support varying cover glass thicknesses and air gaps. Plus, with support for lower interface voltages, it's ready to connect with the next generation of high-integration processors.

As industries push for smarter, more responsive systems, dToF sensors help bridge the gap between simple detection and intelligent interaction. Whether facilitating precision sensing in an automated warehouse or improving gesture control in consumer electronics, they continue to refine the way machines interact with their environment.

To learn more, visit [TMF8806](#).



How low-power overmolded reed switches solve vexing position sensing challenges

By Jeff Shepard

Contributed by DigiKey's North American Editors



Expertise Applied | Answers Delivered

Whether you're designing solutions for automotive, consumer or industrial systems, the space available continues to get smaller. But the challenges, including the needs for low power consumption and high-speed switching of control and position sensing signals, continue to grow. You also need devices that are robust and easy to integrate.

Now, you can turn to the new [59177 Series](#) ultra-miniature overmolded reed switches from [Littelfuse](#) that deliver solid performance with low power consumption in a space-saving configuration and solve vexing design challenges for level monitoring, position sensing, tamper detection, and similar functions. They are suited for diverse applications like security systems, consumer appliances, metering, process monitoring, and battery-powered devices.

Low profile, big performance

The new low-profile design is key. The 59177 series is only 9 mm high, over 20% thinner than the 11.43 mm height of previous reed switches. Overall dimensions of these Form A single-pole single-through normally-open (SPST-NO) switches are 9.0 mm x 2.5 mm x 2.4 mm (0.354"x 0.098"x 0.094") with inward formed J-shaped leads that support compact solutions (Figure 1).

The low profile gives you a new option for solving design challenges in applications that need to switch up to 170 Vdc and up to 0.25 A at 10W, maximum, or 120 Vac and up to 0.18 A, at 10 volt-amperes (VA), maximum. When closed the maximum contact resistance is only 220 mΩ.

Quick reaction times are often needed, and the 59177 series delivers. These switches close in a maximum of 0.5 ms (including bounce) and have a release (opening) time of 0.2 ms, maximum, both according to EIA/NARM RS-421-A.

Even though they can quickly switch high power levels, standby and operating power consumption is zero, so is leakage current when the switch is off, you can't get lower. The 59177 series reed switches can help you maximize the operating time of battery-powered Internet of Things (IoT) designs and meet the most demanding standby power requirements for ac-line operated devices.

Robust and reliable

These switches are rated for operation from -40 to 125°C. The thermoset over mold material enhances the overall robustness and durability, and the inward formed J-shaped leads contribute to improved mechanical resilience and minimize concerns

Figure 1: From the compact package outline to the lead structure, 59177 series reed switches are designed to solve difficult position sensing challenges. (Image source: Littelfuse)

with thermal expansion.

The overmolded design provides excellent mechanical shock and vibration resistance, making it suitable for applications where the switch may experience mechanical stress. You can design these switches into applications with up to 100 G of shock and 30 G of vibration, as specified in EIA/NARM RS-421-A and MIL-STD-202.

The hermetically sealed, magnetically operated contacts ensure reliable operation and protection from the environment. Hermetic sealing also improves switch operation by protecting the contacts from dust and other pollutants that can interfere with the operation of unsealed mechanical or optical switches.

Finally, the hermetic sealing makes them suitable for use in explosive atmospheres where even tiny sparks from conventional switches constitute a hazard. The 59177 series is certified to European standard ATEX (ATmosphères EXplosibles) II 3 G Ex nC IIC Gc.

The ability to operate in harsh environments makes the 59177 series suitable for a wide range of applications. Of course, the ATEX rating can be needed in industrial settings, but if you've ever experienced a door or window slammed shut in a residence, you

know that security devices aimed for use in homes can experience high levels of shock and vibration. The 59177 series excel in those applications as well.

The compact size and no leakage current when open in standby, plus zero operating power consumption of these switches bring huge benefits to battery-powered applications that may never experience harsh shock or vibration, like tamper protection for meters, proximity and limit sensing in small consumer appliances, and some types of process control equipment.

While the general specifications make these reed switches suited for a wide range of applications, the ability to select from several sensitivity levels makes it simple for you to optimize performance for specific design and packaging requirements.

Sensitivity selection

Being able to select the sensitivity of reed switches is a crucial specification since it determines the activation distance and reliability of the switching action, important considerations to ensure optimal performance based on your specific application demands.

Some applications require

sensing and switching to take place at a relatively large distance and need a higher sensitivity device. Reed switches with lower sensitivities are best suited if the application requires a short activation distance.

If the switch is too sensitive, it can experience false triggering from stray magnetic fields or vibrations. If the switch is not sensitive enough, it might not activate when needed. In either case, system reliability suffers.

The basic parameter related to sensitivity is ampere-turns (AT) that measure how close a magnet needs to be to trigger a switch. A low AT indicates a higher sensitivity, and the switch will activate with a weaker magnet of over a greater distance. A high AT switch needs a stronger magnet or closer proximity for operation.

Littelfuse specifies three parameters related to sensitivity. The pull-in AT range measured before molding and modification of the AT. The activate distance range in mm. The deactivate distance range in mm.

The 59177 series offers three sensitivity options denoted by "S", "T", and "U", that correspond with models, 59177-1-S-00-D, 59177-1-T-00-D, and 59177-1-U-00-D, respectively (Table 1).

Select Option		S			T			U		
	Switch Type	Pull-In	Activate Distance (mm)	Deactivate Distance (mm)	Pull-In	Activate Distance (mm)	Deactivate Distance (mm)	Pull-In	Activate Distance (mm)	Deactivate Distance (mm)
		AT Range			AT Range			AT Range		
1	Normally Open	6-10	3.8-5.9	3.6-6.8	10-15	3.0-5.5	3.6-6.3	15-20	2.5-4.6	3.7-5.8

Table 1: The three sensitivity levels of the 59177 series support AT ratings from 6 to 20 making them suitable for a wide range of application requirements. (Table source: Littelfuse)

Simple integration

Littelfuse 59177 series ultra-miniature reed switches are designed to simplify system integration. They are available in cut tape, tape and reel (complies with EIA-RS-481-1) and Digi-Reel formats to fit your specific assembly needs.

They are compatible with pick and place assembly and their ability to operate through non-ferrous materials like wood, plastic, or aluminum, expands application packaging possibilities. They are solder reflow compliant to the IPC-A-610 standard, further ensuring ease of manufacturing and assembly.

The companion model 57045-000 Alnico-5 magnet is in a rectangular 0.700" L x 0.130" W x 0.170" H (17.8 mm x 3.30 mm x 4.32 mm) package with mounting clips to ease installation onto printed circuit boards (Figure 2). The model sensitivities detailed in Table 1 are based on using the 57045-000 magnet.

Alnico-5 magnets are suitable in a wide range of applications and offer a balance of strength and temperature stability. They maintain their magnetic properties even at high temperatures, model 57045-000 is rated for operation at ambient temperatures up to 105°C, and they are corrosion resistant, making them ideal for use in harsh environments.

Conclusion

Everything about the Littelfuse 59177 series reed switches simplifies your tasks when

addressing vexing position and motion sensing challenges. They can switch up to 10 W, are hermetically sealed against harsh environments, and are mechanically robust. Their zero standby and operating power consumption is perfect for both battery-powered IoT and ac-powered applications. Finally, they're designed to simplify system integration and support automated assembly.



Figure 2: This 57045-000 Alnico-5 magnet is optimized for use with 59177 series reed switches and clips directly into the circuit board for quick and easy assembly. (Image source: Littelfuse)



How A2L sensors make sure refrigerants don't blow(up)

What HVAC engineers need to know about A2L

The HVAC industry is no stranger to design trade-offs. In fact, it is staring down an industry-wide redesign thanks to the adoption — and trade-offs — of A2L refrigerants.

Historically, refrigerants have been harsh on the environment. This led to the phaseout of formulations with high ozone depletion potential (ODP). Since the phaseout started in the early 2000s, the UNEP estimates that the ozone layer will fully recover by mid-century.

Unfortunately, these replacement refrigerants came with a price — global warming potential (GWP). Even newer refrigerants are now destined to replace those with high GWP, but they also come with a price — flammability. But don't be alarmed; [engineers are designing modifications to HVAC systems, standards, and procedures to ensure everyone's safe, and the only things that blow are the fans.](#)



The history of HVAC refrigerants and their effects on the environment

A substance's impact on global warming is calculated relative to the greenhouse effect of carbon dioxide (CO₂). Thus, the GWP of one ton of CO₂ is one ton of CO₂-equivalent, often shortened to just: 1.

The global warming potential of R-410, a popular refrigerant scheduled to be phased down, is 2,088. In other words, the impact of one ton of R-410 released into the atmosphere would be equal to releasing 2,088 tons of CO₂.

According to newer regulations, the maximum allowable GWP for a refrigerant will be 700.

This has led to ASHRAE redefining its refrigerant safety classifications to enable the adoption of A2L refrigerants. This classification previously categorized refrigerants into six buckets defined by:

- A letter: where A denotes low toxicity and B means highly toxic.
- A number: where 1 means not flammable, 2 is flammable and 3 denotes highly flammable.

Thus, refrigerants were easily identified to be flammable and/or toxic based on their classifications: A1, A2, A3, B1, B2, or B3. The redefined classification adds a second letter and two more buckets: A2L and B2L. Here, the L denotes that the refrigerant is flammable but with a low burning velocity.

A few A2L refrigerants are vying to become the new standard refrigerants in the industry — based on their GWP. The current top contenders are R-32 with a GWP of 675 and R-454B with a GWP of

467. And though the risks of these refrigerants igniting are minor, engineers must maximize safety by ensuring HVAC systems are equipped with the tools to detect and react to refrigeration leaks.

How flammable are we talking? And how engineers must respond.

For a refrigerant to be classified as A2L or B2L, it must have a burning velocity lower than 10 cm/s (3.9 in/s). Though these materials will ignite, many tests have shown they tend to self-extinguish. Additionally, the gases must be highly concentrated to ignite as they have a lower flammability level of 300g/m³ (10.8 lb/in³). Though it's best to avoid sparks and flames, many A2L refrigerants have been assessed to be safe around some — but not all — common ignition sources.

So, A2L refrigerants can and will ignite under various conditions. As a result, many of the 'best practices' used around A1 or B1 refrigerants — like purging and evacuating lines — become mandatory when working with A2L or B2L refrigerants.

HVAC Engineers working with A2L refrigerants will also need to implement safety equipment into their systems designs as per UL

60335 2-89 standards. For instance, they will need to integrate sensors and control boards that can detect and appropriately respond to a refrigerant leak. Specifically, they will need to add sensors that can sniff out A2L gas and message HVAC control boards so the system can:

1. Shut off the circulation of the refrigerant to stop it from pooling.
2. Shut off all potential ignition sources around the leak.
3. Blow air into where the leak is detected to reduce the chance of ignition.

Engineers and technicians working around A2L refrigerants will also need to pay better attention to the tools they use. For instance, any power supply, drill or light source must be labeled A2L compatible if they are to be used in proximity to these refrigerants.

Again, all these precautions have remained best practices within the HVAC industry. For instance, any refrigerant leak should be avoided, or quickly detected, to:

- Maintain maximum efficiency of the HVAC system.
- Meet OSHA exposure limit regulations.
- Maintain proper charge, performance, and operations.

So, many engineers and technicians will hardly notice a change to their workflows, whereas anyone who took advantage of the 'timesavers' available when working with A1 refrigerants must change those habits.

A2L gas sensors and control systems

Engineers need sensors that are capable of detecting A2L refrigerant leaks to ensure the safe transition of the HVAC industry towards these more environmental materials. Fortunately, the HVAC industry is not the first to make this transition; most automotive vehicles already utilize A2L refrigerants. Therefore, HVAC engineers have access to tested equipment and procedures to ensure their future success.

For instance, consider Sensirion thermal conductivity CMOSens MEMS chip series — which contains the SGD43S-M3-S5 and SGD43S-M3-S7. They have already been used around the world for automotive and medical sensor applications.

The sensor detects A2L gases using thermal conductivity. As a result, it is protected from common sensor issues like contamination, poisoning, drift, and the degradation of mechanical

components. Sensirion sensors are reported to have a 15-year lifecycle. During that time, the sensor will not need to be recalibrated or rezoned.

The SGD43S-M3-S5 and SGD43S-M3-S7 sensors are capable of producing dual contact relay output so they can trigger a signal to a control board. The board can then start a blower, switch off heat sources, and stop the flow of refrigerant within the system. Technicians can also use the LED on the sensor to quickly detect its status. Finally, the sensors meet current industry standards like UL 60355-2-40 and UL 60335-2-89, so they are ready to use.

The main difference between the SGD43S-M3-S5 and SGD43S-M3-S7 is the refrigerants they are calibrated



The Sensirion thermal conductivity CMOSens MEMS chip series, containing the SGD43S-M3-S5 and SGD43S-M3-S7, can detect A2L leaks and ensure the safety of HVAC systems. (Image: Sensirion AG, DigiKey.)

to detect. The S5 model is calibrated for R-454B and R-32, so it is already primed to work with the two leading A2L refrigerants in the HVAC industry. The S7 model, however, is calibrated to detect R-454A, R-454C, and R-455A and is thus more useful in refrigeration applications.

For more information on the SGD43S-M3-S5 and SGD43S-M3-S7 and how they can be integrated into HVAC and refrigeration systems, [read this product page on DigiKey.com.](#)

Come to your sensors

DigiKey

We stock a huge range of top quality environmental and positioning sensors.

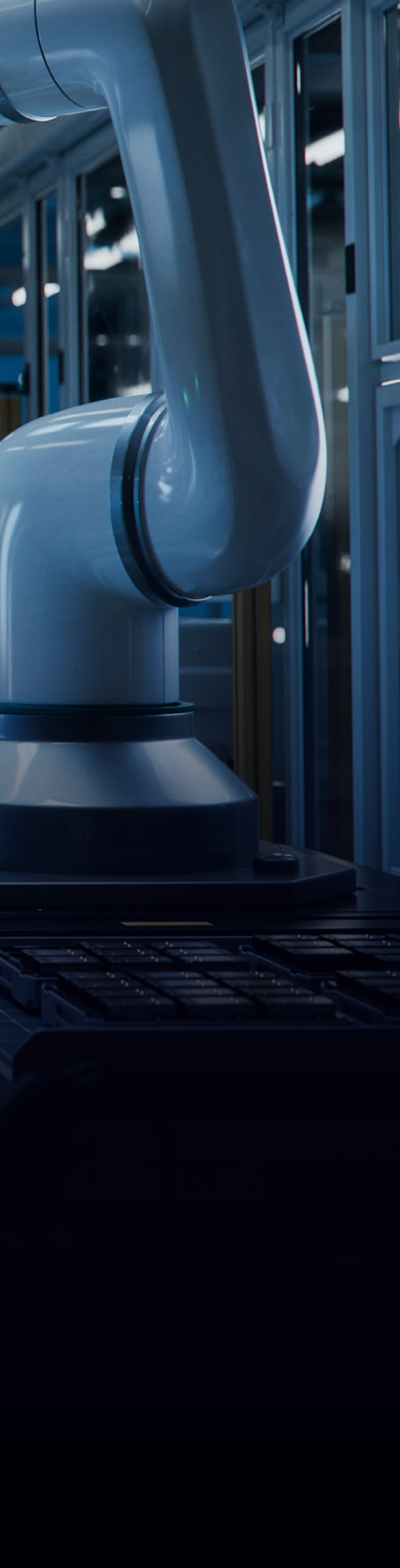
[Learn more](#)



The background of the image shows a modern industrial factory floor. Several white robotic arms are visible, positioned over a workbench. The lighting is cool and blue, creating a high-tech atmosphere. The robotic arms are sleek and have green and red accents near their joints. They appear to be working on a complex assembly, possibly electronic components or small mechanical parts. The perspective is from a low angle, looking up at the robots, emphasizing their scale and precision.

Advancing magnetic sensing with Allegro MicroSystems' Tunnel Magnetoresistance (TMR) technology

By Allegro MicroSystems



From the automobiles we drive and the factories that power our economy to the smartphones in our pockets and the medical devices that save lives, magnetic sensors are crucial components used to sense position, speed, and current. However, with the increasing demands of emerging applications, standard magnetic sensors have reached their limits. To achieve greater accuracy, lower power consumption, and improved reliability, an improved type of sensor is required. This article explores the principles of tunnel magnetoresistance, sensors that use this phenomenon, as well as performance benefits over previous magnetic sensing technologies.

The evolution of magnetic sensing

Hall effect sensors, which have been widely used for decades, operate on the effect discovered by Edwin Hall in 1879, which states that whenever a current-carrying conductor is placed in a magnetic field, it produces a voltage difference that is perpendicular to the current and magnetic field. While hall effect sensors are cost-effective components, their sensitivity is typically limited, making them unsuited for applications that demand high precision and the ability to detect weak magnetic signals.

Anisotropic magnetoresistance (AMR) sensors, another common technology, exploits the anisotropic magnetoresistance effect to achieve higher sensitivity compared to Hall effect types. In AMR sensors, the electrical resistance of a ferromagnetic material varies, based on the angle between the current flow and magnetization direction. While AMR sensors have higher sensitivity compared to Hall effect types, they typically have a lower signal-to-noise ratio (SNR). These sensors can also consume more power than Hall effect sensors, which can limit their suitability for low-power applications.

Giant magnetoresistance (GMR) sensors, a more recent development, comprise multiple layers of ferromagnetic materials separated by thin non-magnetic layers. The resistance of this sensor changes significantly when exposed to an external magnetic field, allowing for higher sensitivity and improving the signal-to-noise ratio compared to hall effect and AMR sensors. GMR sensors have been applied in various products, including hard disk drives, automobiles, and biosensors. On the downside, however, depending on the application GMR sensors consume more power and are susceptible to external interfering magnetic fields.

To overcome the performance limitations of these magnetic sensor solutions, engineers can opt for advanced magnetic technologies like tunnel magnetoresistance (TMR) sensors, which offer higher sensitivities, improved power efficiency, thermal stability, and robustness.

How tunnel magnetoresistance (TMR) technology works

Tunnel Magnetoresistance technology harnesses principles of quantum mechanics for accurate magnetic sensing. TMR sensors have a magnetic tunnel junction (MTJ) – a nanoscale structure that is composed of dual ferromagnetic layers separated by an ultra-thin insulating barrier. This insulating barrier, typically made of crystalline magnesium oxide (MgO) and a few atomic layers thick, allows electrons to tunnel through it quantum-mechanically.

In classical physics, an electron cannot pass through an insulating barrier. However, in quantum mechanics, there is a slight probability that an electron can tunnel through the barrier, even if its energy is lower than the barrier height. This tunneling depends on the relative orientation of the magnetization in the two ferromagnetic layers of the MTJ.

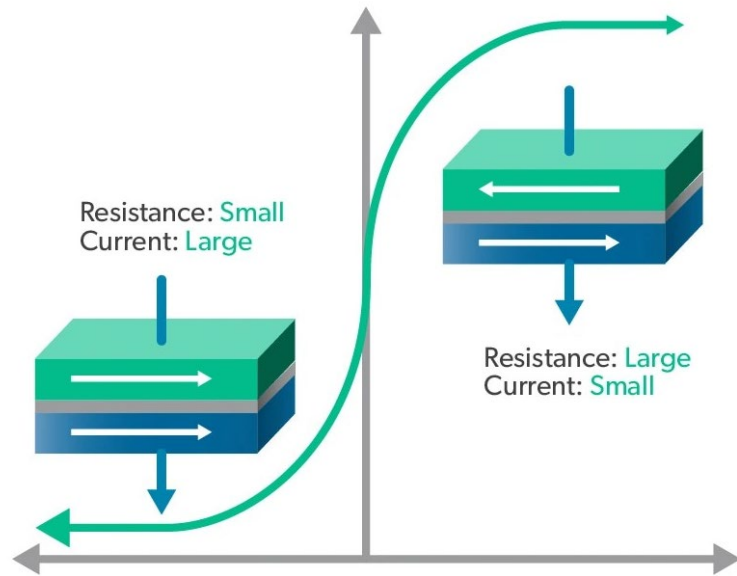


Image credit: Allegro MicroSystems blog

When the magnetizations of the ferromagnetic layers are parallel, the electrons in the majority spin state of one layer can easily tunnel into the majority spin state of the other layer, resulting in a low-resistance state. Conversely, when the magnetizations are antiparallel, electrons in the majority spin state of one layer must tunnel into the minority spin state of the other, leading to a high resistance. This change in resistance, called the “TMR effect,” is larger than the resistance change in other magnetic sensors, allowing TMR sensors to detect even the weakest magnetic fields precisely.

The Magnetoresistance Ratio (MR) quantifies the performance of a TMR sensor by calculating the

percentage change in resistance between the parallel and antiparallel magnetization states. TMR sensors achieve MR ratios of over 200%, significantly higher than those of AMR and GMR sensors, with MR ratios of less than 10% and 20%, respectively. This high MR ratio translates to improved sensitivity, which allows TMR sensors to detect very weak magnetic fields.

Another advantage of TMR and GMR sensors are their compatibility with standard semiconductor manufacturing processes. The sensors can be fabricated with advanced thin-film deposition techniques, such as sputtering and molecular beam epitaxy, and incorporated with other components on a single

chip. This compatibility enables manufacturers to design compact, low-power, and cost-effective TMR sensors that are suitable for a broad range of applications.

Advantages of TMR over other magnetic sensing technologies

TMR sensors exhibit remarkably high sensitivity, with the ability to detect magnetic fields as low as a few microTesla. This high sensitivity is a result of the larger MR ratio achievable in TMR sensors, which can

exceed 200%. In comparison, AMR sensors typically have MR ratios of less than 5%, while giant magnetoresistance (GMR) sensors have MR ratios of around 10-20%.

TMR sensors also operate at extremely low power levels, consuming less power compared to AMR and GMR sensors. This low power consumption is due to the high resistance of the MTJ and the low current required for sensing. For example, TMR sensors can utilize supply voltages as low as 1V and consume a small amount of current, making them highly energy efficient. This makes

these sensors useful in battery-powered applications such as wearables and IoT nodes, where extended battery life and low energy footprint are critical.

TMR sensors exhibit excellent linearity, meaning that the sensor output is directly proportional to the applied magnetic field over a wide range. This linearity is a result of the well-defined, stable magnetic response of the MTJ, which is governed by the quantum mechanical tunneling process itself. The linear responses of TMR sensors simplify the calibration process and ensure

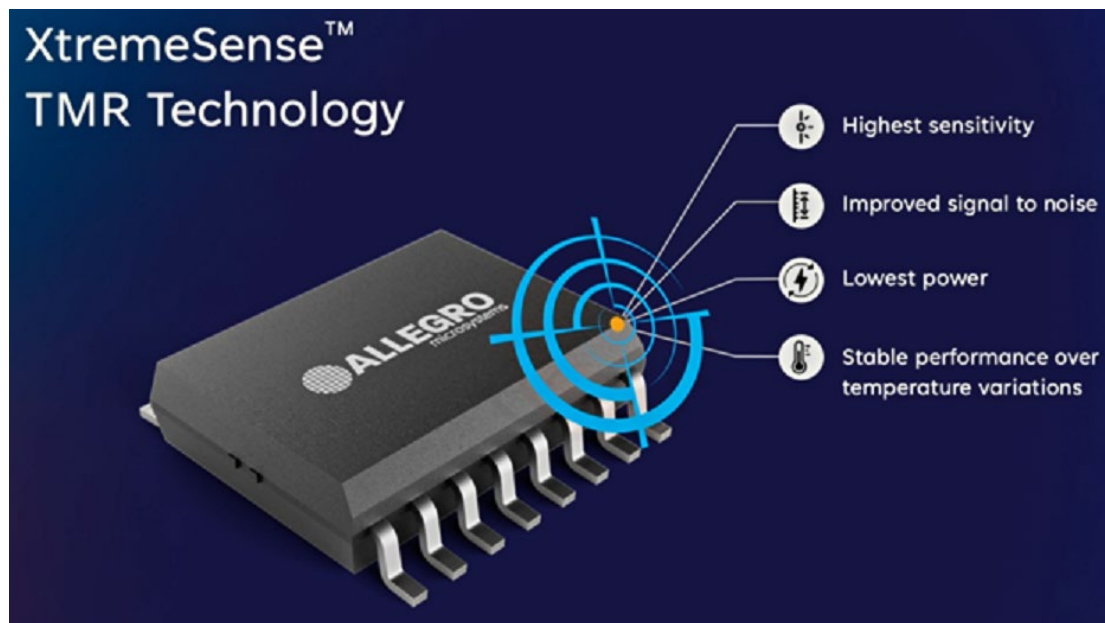


Image credit: Allegro MicroSystems

that measurements are accurate, without the need for complex compensation algorithms.

In terms of thermal stability, TMR sensors offer a stable performance over a broad temperature range, typically from -40°C to 150°C. The stable performance of these sensors ensures reliable operation in harsh environments, such as automotive and industrial applications, where sensors can be exposed to extreme temperatures and temperature fluctuations.

Product highlight: Allegro MicroSystems' XtremeSense TMR sensors

Lastly, TMR sensors are inherently robust and reliable, with a solid-state design that eliminates moving parts and reduces the risk of mechanical failure. For example, the MTJ structure itself is resistant to mechanical stress, vibration, and shock. TMR sensors also demonstrate resistance to radio frequency interference, making them suitable for noisy electrical environments.

Allegro MicroSystems' [XtremeSense TMR portfolio](#) includes a wide range of sensors optimized for various applications ranging from position sensing to high-bandwidth current

measurements. These sensors leverage the inherent benefits of TMR technology, such as higher sensitivity, low power consumption, wide dynamic range, and industry-leading performance over a temperature range from -40°C to 150°C.

[XtremeSense Crocus Technology](#)
TMR sensors incorporate sophisticated signal conditioning and digital processing (DSP) capabilities to improve sensor performance and ease of use. Signal conditioning circuits, such as low-noise amplifiers and filters, amplify and process the sensor output to reduce SNR and minimize the effect of external noise. These circuits have been carefully designed to match the characteristics of the TMR sensor, ensuring optimal performance and signal integrity.

Allegro TMR technology uses differential sensing to reject stray fields, this ensures stable and reliable sensor performance in a broad range of operating conditions. This technology is crucial in applications where sensors are exposed to strong magnetic fields or where multiple sensors will be placed in close proximity, as it prevents crosstalk and interference.

In addition to EMI shielding, Allegro's unique packaging allows for multiple sensors and

signal conditioning circuitry to be built into a single package. This integration simplifies system design, reduces the overall footprint, and improves signal integrity. By combining the TMR sensor with advanced signal conditioning and processing circuitry, XtremeSense sensors minimize the need for external components and reduce the design complexity for engineers.

TMR also includes digital interfaces, such as I2C and SPI, which allows them to be integrated with microcontrollers, digital signal processors, and other digital systems for easy configuration, control and data readout from sensors. These interfaces have advanced features like programmable gain settings, filtering options, and self-calibration, offering designers greater flexibility and control over sensor performance.

Key applications

In the automotive sector, TMR sensors are instrumental in enabling advanced driver assistance systems (ADAS) to enhance vehicle safety and performance. For example, these sensors can be used for position sensing in electric power steering systems, providing accurate feedback on steering



Image credit: Allegro MicroSystems

angle and enabling smooth and responsive steering control. Other applications include pedal position detection for accurate throttle and brake control and transmission gear selection. This technology can also be used in motor control and battery management to provide current measurements to optimize the performance of motors and ensure efficient charging and discharging of vehicle batteries.

In industrial applications, TMR sensors can provide accurate position feedback in servo motors and linear actuators for motion control and positioning in manufacturing systems, pick-and-place machines, and other

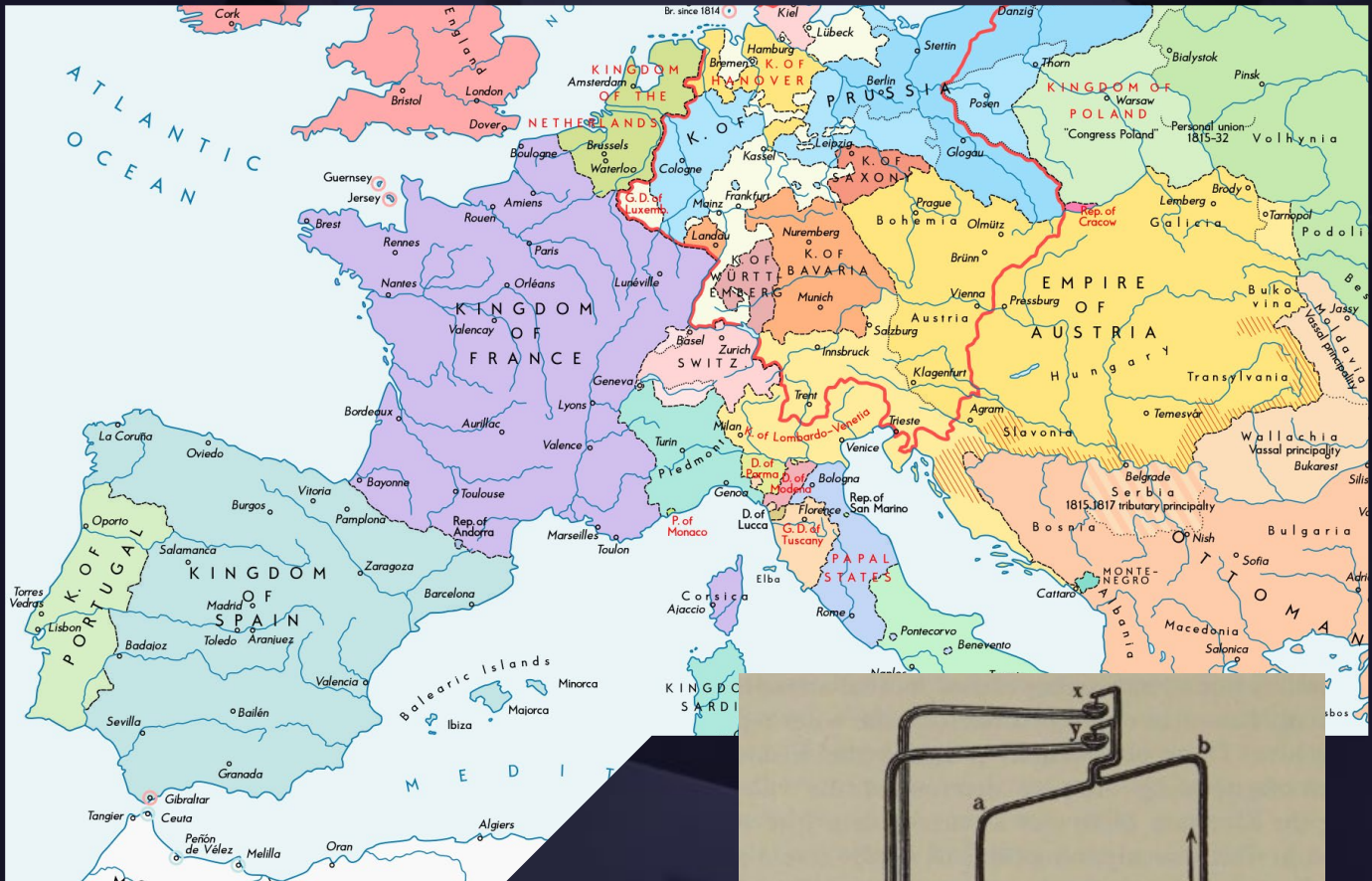
automated equipment. Current sensing is also essential for industrial applications for motor protection, power monitoring, and energy management. Here, TMR sensors can provide precise current measurements for real-time monitoring of motor health, detection of overload conditions, and optimizing energy consumption.

TMR sensors can also be integrated into consumer products like gaming devices and smartphones to provide new features and enhanced user experiences. For example, these sensors can provide gesture recognition allowing users to interact with devices

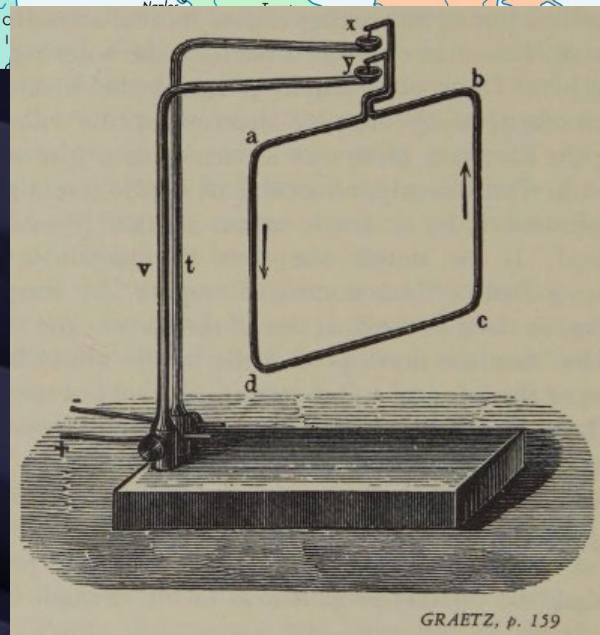
through intuitive motion controls. Other applications include motion tracking and orientation detection for more immersive gaming experiences and advanced user interfaces.

Conclusion

TMR technology is a breakthrough in magnetic sensing that offers better performance, energy efficiency, and reliability compared to standard magnetic sensors. With their high sensitivity, low power consumption, temperature stability, and wide dynamic range, these sensors are able to meet the current and future needs of various industrial, automotive, and consumer applications.



This is a map of Europe as it was when the galvanometer was invented.



An illustration the test tool that Ampere devised when investigating electromagnetism.

Experiments on the effect of a current of electricity on the magnetic needle

By David Ray
Cyber City Circuits

The Galvanometer

At the turn of the nineteenth century, electricity was still a mysterious force—poorly understood, difficult to measure, and often viewed with wonder or suspicion. Scientists exploring electricity needed precise instruments capable of detecting even the faintest currents, laying the groundwork for the invention of a device that would revolutionize both scientific study and industrial development: the galvanometer.

The name 'galvanometer' is rooted in the intriguing experiments of Luigi Galvani, an Italian physician and physicist who, in the late 18th century, famously observed the twitching of frog legs when subjected to electrical current—what he termed "animal electricity."

Galvani's experiments ignited a sensation across Europe, capturing public imagination and fueling intense scientific curiosity. His work prompted Alessandro Volta to create the first 'reliable' electric battery (the voltaic pile), which in turn enabled Hans Christian Ørsted, André-Marie Ampère, and Georg Simon Ohm to perform groundbreaking experiments that fundamentally reshaped human understanding of electricity.

The story that led to the galvanometer is part of a much larger story that shows how connected Europe was. From 1820 through the end of the nineteenth century, the rapid pace of discovery and invention rivaled the semiconductor boom in the latter half of the twentieth century.

This chain reaction of discoveries led directly to the development of the galvanometer, an instrument initially intended simply to detect and measure small electrical currents but soon found indispensable applications in fields as diverse as medicine, telegraphy, and physics.

The birth of the Modern Age

The late 1700s was a significant turning point for society. Even the ancient Greeks knew about electricity, but nobody knew what it was or where it came from. By then, people were able to generate electricity by using giant spinning contraptions that would rub small leather cushions onto large glass globes. The faster the 'electrical machine' spun, the more electricity

it produced. Sometimes, these machines produced so much high-voltage current that they fatally electrocuted onlookers.

In 1745, the elegant invention of the Leyden jar was introduced, giving the world a way to actually store electricity. Before, any charge from the machines would quickly dissipate. Now that a charge could be stored, it could be studied. The field would stagnate until Benjamin Franklin's 1752 kite experiment turned many doctors, mechanics, and natural philosophers into hobbyist electrical engineers. Newspapers around the world published detailed instructions on how to construct a kite from two cedar sticks and a silk handkerchief. There are accounts of hundreds of people successfully recreating the experiment within months of Franklin publishing it.



'Using complex machines that spin glass and can generate thousands of volts of electricity was the best method for studying electricity.'

Franklin's experiments resulted in the practical use of the lightning rod, which not only made people safer but also allowed both amateurs and professionals to study electricity easier when combined with large Leyden jars.

In 1800, Alessandro Volta invented the voltaic pile. This device was simple: alternating discs of two different metals, typically copper and zinc, separated by layers of cloth or paper soaked in saltwater or acid, which acted as an

Retro Electro Fun Fact: The Leyden Jar was independently invented by Pieter van Musschenbroek in Leiden, Netherlands. It could store an electrical charge in a way similar to a capacitor, with dual conductors, and a dielectric in the form of a glass jar. The jar was filled with water or brine and sometimes beer. Not at all understanding what he had made, Musschenbroek thought the electrical fluid (effluvia) was being injected and stored within the water which was later omitted altogether. Learn more about electrical effluvia in the Retro Electro article 'Electricity or Ethereal Fire.' (Link: <https://emedia.digikey.com/view/785457150/28-29/>)

electrolyte. Stacked in layers, this arrangement produced a stable, continuous electric current, unlike earlier electrostatic machines or Leyden jars, which could only deliver brief bursts of electricity and could never provide any consistency.



Benjamin Franklin's kite experiment really gave the field of study a kick start in the 1750s

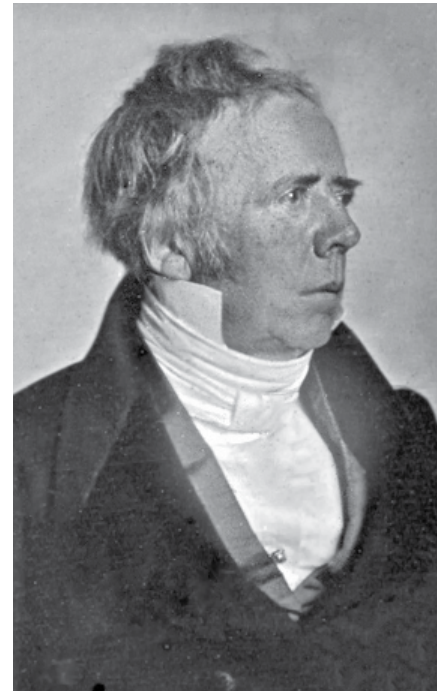
The period between the late 1700s and 1820 was ripe for discovery in electricity. Finally, an experimenter could have a constant and reliable source of electricity. For the most part, few among the many experimenters had any idea what they were doing. There are stories of people tying lightning rods to elephants and other large animals.

Italian doctor Luigi Galvani found that you can connect a Leyden jar to dead animals and make them jump around. Traveling doctors were roaming rural New England, treating everything from asthma to dysentery with electric shock. Humphrey Davy was about to isolate several elements (calcium, magnesium, potassium, sodium) for the first time with electrolysis. ...and in the Netherlands, Hans Christian Ørsted started his investigation of electricity.

Hans Christian Ørsted

Ørsted was a brilliant mind. He grew up on an island off the coast of Denmark called Langeland. There was no formal school, but community members would take time to teach children arithmetic, drawing, and languages like German and French from people like the town's mayor. He attended the University of Copenhagen and received a PhD in 1799.

Soon after the invention of the voltaic pile was published, he began conducting his own experiments as a young man. He spent a few years traveling Europe to study with other researchers. At the time, people suspected a connection between magnetism and electricity, but nobody could find it. It sounds simple today, but researchers



Hans Christian Ørsted

would put a compass needle near batteries, Leyden jars, and high-voltage wires, and the connection could not be made.

While teaching a class and demonstrating that a wire will produce heat when connected to a battery, he noticed that a nearby compass fluttered when the battery was connected. After meticulous experimentation, all he could come up with was that there was a clear connection between electricity and magnetism when a very high current was run through a wire. He found that a compass needle will deflect perpendicular to the conductor, demonstrating that the

Writer's Note: While researching, the writer found numerous references to gossip and experiments concerning the connection between electricity and magnetism. It appears that the wire and compass experiment had been conducted for decades before Ørsted's discovery. The writer hasn't found what made those experiments unsuccessful. An Italian researcher named Gian Domenico Romagnosi published a study on the connection between static buildup and the movement of a compass needle in 1802, but it seems that his research didn't disseminate widely across Europe.

magnetic field the coil generates travels around the wire and not through it, like everyone assumed.

The problem now is that nobody knew how to describe this observation in practical mathematical terms. Ørsted

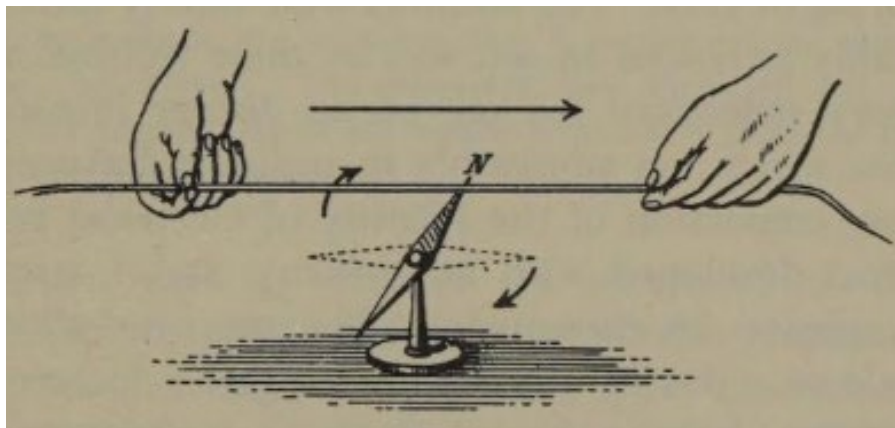
experimented for months and then published a short paper in Latin titled '*Experiments on the Effect of a Current of Electricity on the Magnetic Needle.*' Papers like this took some time to travel and get translated through Europe.



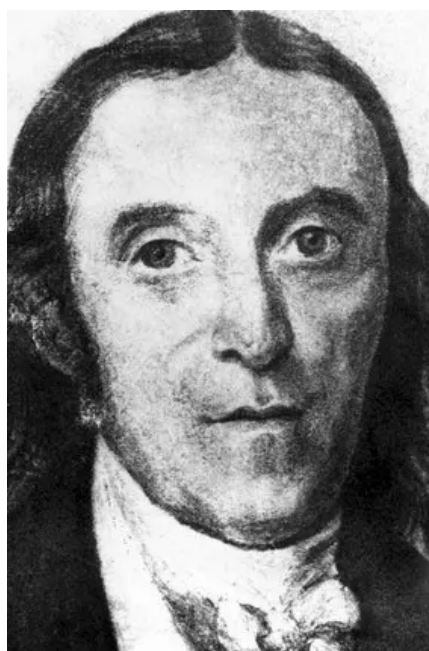
FIGUIER, p. 713

Lecturing before a select group of students, Oersted, in the spring of 1820, noticed that the needle of a nearby magnetic compass deviated when the circuit of a voltaic pile was completed. On July 21 the discovery of electromagnetism was announced.

In the spring of 1820, during a lecture, Ørsted discovered evidence linking magnetism to electricity.



This image illustrates the simple demonstration performed by Ørsted that initiated the modern age.



Johann Salomo Christoph Schweigger

J o u r n a l
f a r
C h e m i e u n d P h y s i k
i n V e r b i n d u n g

As the discovery traveled Europe...

In Bavaria...

In the Summer of 1820, Johann Schweigger was sitting at his desk when the Dutch journal that first published Ørsted's discovery came in the post. Schweigger was the editor and publisher of the German scientific journal '*Journal für Chemie und Physik*' (often known simply as '*Schweigger's Journal*'). He was uniquely positioned to be one of the first in the world to learn about new scientific discoveries.

Recognizing the significance of Ørsted's experiment, Schweigger immediately saw the potential to measure electric currents with precision. Schweigger first determined that the fields

created by current in a wire could be 'multiplied' by coiling the wire. He coiled wire around a wooden rectangular frame and placed a compass needle in the center. By the fall of 1820 (just months after Ørsted's paper appeared), Schweigger constructed his 'Multiplier Galvanometer,' also called 'Schweigger's Multiplier.' In September of 1820, Schweigger presented his findings at the University of Halle (where he was also a teacher). Soon after, his paper was published in the German Literary Gazette, eventually showing up on the desk of every academic physics researcher in Europe.



This is a depiction of the Schweigger Multiplier.

In France...

A French physicist named Francois Arago found a copy of Ørsted's paper while visiting Geneva and brought it back to Paris to be published in the French scientific journal *Annales de Chimie et de Physique*. In September 1820, he demonstrated the experiments to an audience in Paris, including the mathematician and chemist André-Marie Ampère.



François Arago

Excited by the challenge of explaining the movement of the needle, Ampère dedicated his energy to solving it. Already a highly distinguished mathematician, chemist, and philosopher, he pursued problems that captivated him. He struggled with severe and

chronic depression. While a genius, he could only 'work at 100 MPH' or not at all.

When Ampère learned of Ørsted's discovery, he immediately set out to investigate in hopes of mathematically explaining this new connection between electricity and magnetism. Remember, that the connection was suspected by many, but nobody had reproducible evidence of such a connection until now. Within a week, Ampère conducted a series of experiments and presented his initial report to the French Academy of Sciences just days after Arago published the discovery.

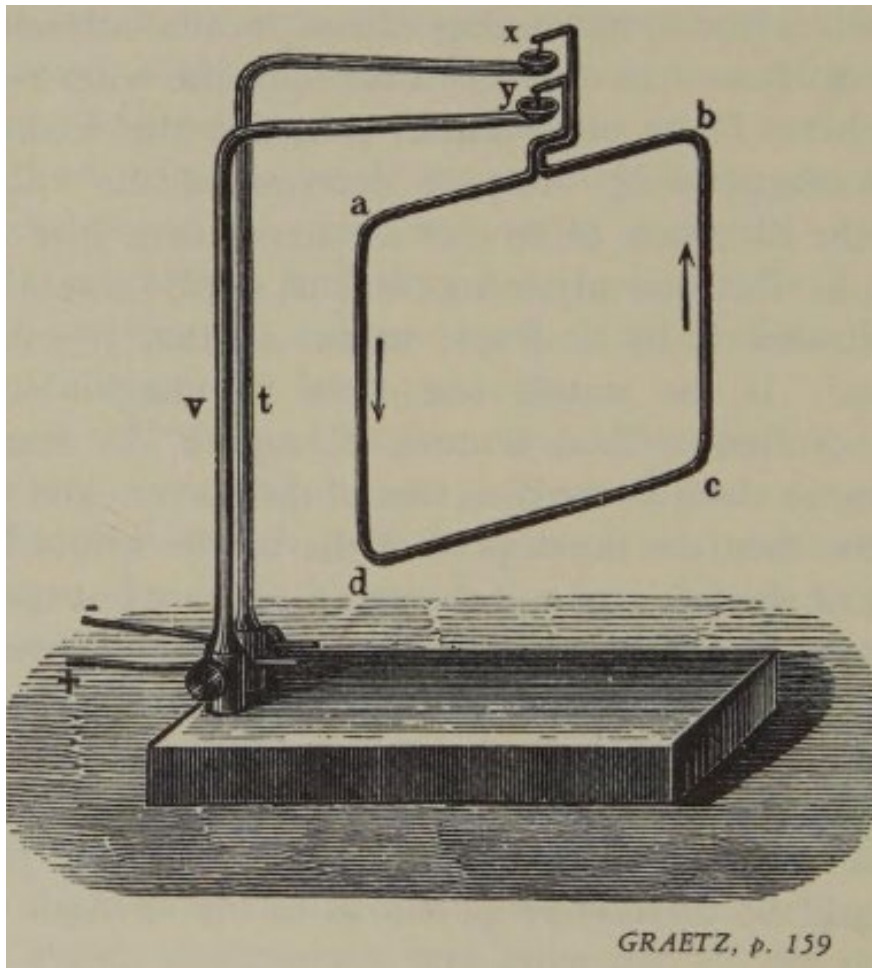


André-Marie Ampère

Retro Electro Sad Fact:
Did you know that French revolutionaries beheaded Ampère's father while Ampère was a teenager? Read that story and more in the Retro Electro article 'Genius and Tragedy.' (Link: <https://emedia.digikey.com/view/687420822/38/>)

Ampère discovered that two parallel wires carrying electric currents either attract or repel each other, depending on the direction of the current. This critical finding demonstrated that electricity creates magnetic effects not only on compass needles but also directly between wires.

Ampère introduced the first detailed mathematical proof of electromagnetism, now known as Ampère's Law. It states that 'the magnetic field created by an electric current is proportional to the size of that electric current with a constant of proportionality equal to the permeability of free space (air).' For the first time



An illustration the test tool that Ampere devised when investigating electromagnetism.

there was a mathematical proof for the connection between electricity and magnetism. Over the next couple of years, he published more findings on this phenomenon, ultimately creating the field of study known as electrodynamics (électrodynamique). In his 1873 book 'A Treatise on Electricity and Magnetism,' James Clerk Maxwell built upon and refined his work.

In Prussia...

A Bavarian school teacher in Cologne bought a copy of Schweigger's Journal in the summer of 1820. Georg Ohm was teaching mathematics and physics at the Jesuit Gymnasium at the time. This gave him the use of well-equipped laboratories and ensured early access to scientific journals, letters, and

European science news. Over the next five years, Ohm performed comprehensive electrical circuit experimentation using the Schweigger Multiplier, leading to his 1827 publication of 'The Galvanic Circuit Investigated Mathematically' ('Die galvanische Kette, mathematisch bearbeitet'). This work led to 'Ohm's Law' describing the mathematical proportions between tension (voltage), intensity (current), and reluctance (resistance) allowing for proper metering when applied to the galvanometer's operation.

Retro Electro Fun Fact: The galvanometer, with several enhancements from many others of the day, enabled a form of measurement. Suddenly, there could be standards, and numerous ones emerged. Read more about the story of the first internationally recognized unit of electrical resistance in the Retro Electro article 'Ohm's Day.' (Link: <https://emedia.digikey.com/view/639112496/21/>)



Georg

In Britain...

Arago's demonstration in early September 1820, was quickly reported to the science community within Britain. Notably Sir Humphry Davy and his lab assistant, Michael Faraday. Davy was the President of the Royal Society at the time, a seat that was held by Sir Isaac Newton a hundred years earlier. He and Faraday's research culminated in 1831, where Faraday proved that not only does a current create magnetic fields, but magnetic fields can create a current. His discovery of electromagnetic induction led to his invention of the electric generator.

Legacy

The galvanometer may very well be the most important tool to emerge from the nineteenth century. With the practical application of Ørsted's research, it had an impact throughout Europe within weeks. Although Europe was divided by language, this story illustrates how the publication of periodic research journals could translate and disseminate milestone discoveries in just a matter of weeks. This narrative also shows that, despite the efforts of the brightest minds on the planet to find a connection between magnetism and electricity, it took decades for a single observation to be documented and reproduced, triggering the electrical boom and paving the way for the second industrial revolution.



Sir Humphrey Davy

1745

Pieter van Musschenbroek invents the **Leyden Jar** in Leiden, Netherlands, allowing electricity to be stored.

Late 1700s

Electrical machines capable of generating static electricity become popular, although dangerous and inconsistent.

Luigi Galvani conducts experiments with frog legs, demonstrating "animal electricity," sparking scientific curiosity about electricity and galvanism.

1802

Gian Domenico Romagnosi publishes research on electricity affecting compass needles, but his findings are not widely recognized.

Summer 1820

Johann Schweigger in Bavaria reads Ørsted's paper and invents the Multiplier Galvanometer, significantly enhancing the measurement of electrical currents. He presents his findings in September 1820 at the University of Halle.

1820-1825

Georg Simon Ohm, working in Cologne, utilizes Schweigger's galvanometer for detailed studies on electricity, leading him to formulate **Ohm's Law** in 1827.

1831

Michael Faraday, working with Humphry Davy in Britain, discovers electromagnetic induction, leading directly to the invention of the electric generator.

1752

Benjamin Franklin conducted the famous kite experiment, which demonstrated that lightning is electricity. This experiment significantly increased public interest in electrical experimentation.

1800

Alessandro Volta invents the **Voltaic Pile**, providing a reliable and continuous source of electricity.

1820

Hans Christian Ørsted observes that an electric current causes a compass needle to deflect, establishing the relationship between electricity and magnetism.

Ørsted publishes his work as *"Experiments on the Effect of a Current of Electricity on the Magnetic Needle."*

September 1820

François Arago demonstrates Ørsted's discovery in Paris.

André-Marie Ampère sees Arago's demonstration and begins experimenting intensively, rapidly producing his first results explaining electromagnetism mathematically.

1827

Georg Simon Ohm publishes *"Die galvanische Kette, mathematisch bearbeitet,"* mathematically describing voltage, current, and resistance.

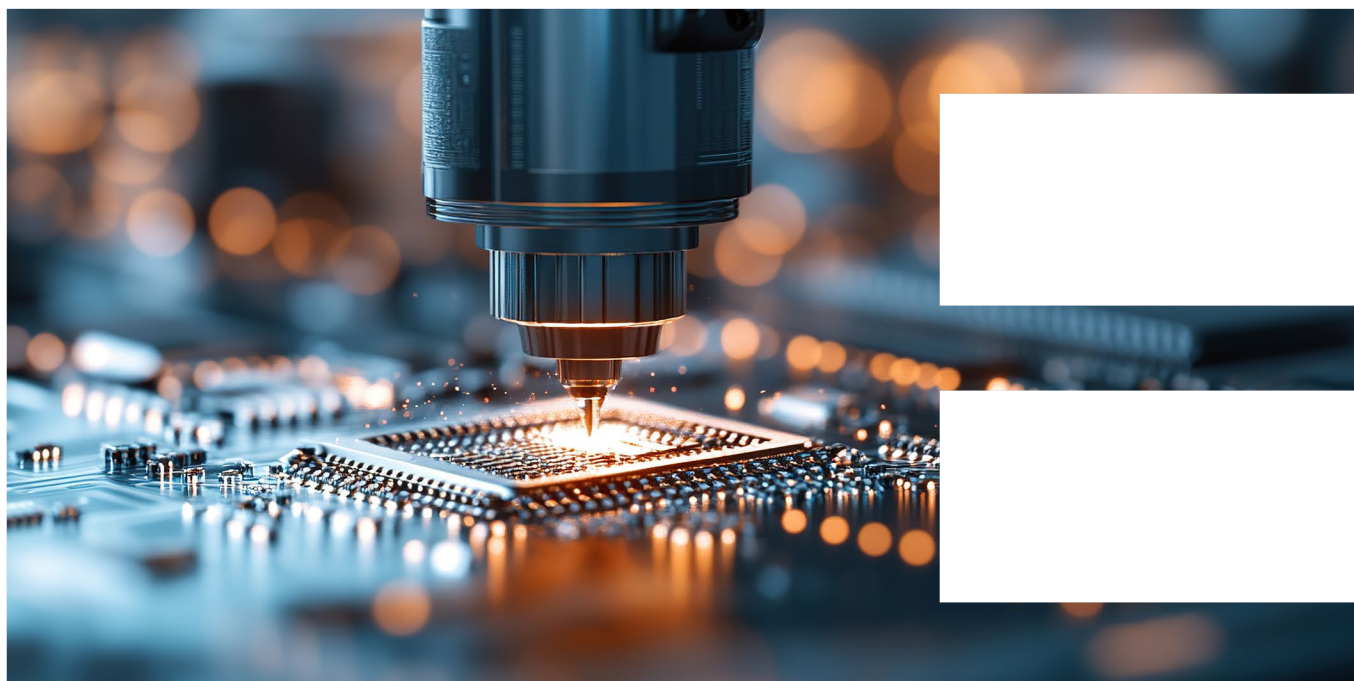
1873

James Clerk Maxwell expands upon Ampère's and Faraday's works in *"A Treatise on Electricity and Magnetism."*

ADI's data acquisition solution shines in advanced lithography chip manufacturing

By Pete Bartolik

Contributed By DigiKey's North American Editors



The semiconductor manufacturing equipment (SME) market is projected to experience substantial growth over the next five years, driven by the anticipated increase in semiconductor chip sales from \$600 billion in 2022 to \$1 trillion in 2030. Sensors are at the heart of the advanced lithography systems used in chip manufacturing.

Manufacturing the complex, high-performance—and ever smaller—semiconductor chips is largely reliant on highly precise and sensitive lithography processes that are instrumental in printing intricate patterns onto silicon wafers and other substrates used in chip manufacturing.

Advanced lithography systems employ extremely accurate and

sensitive techniques, which not only enhance process yield but also minimize waste and optimize plant efficiency. To achieve the sub-micron and nanometer precision essential for mass producing integrated circuits (ICs), these systems rely on thousands of sensors for monitoring and controlling position, temperature, energy, and motion.

Overall system performance relies on the precise and repeatable performance of each individual sensor. Advanced algorithms interpret large volumes of sensor data and coordinate the necessary tweaks in very minor but detailed ways using thousands of actuators.

[Analog Devices, Inc.](#) (ADI) leverages its signal chain

micromodule (μ Module®) technology to provide a high-performance, miniaturized, analog-to-digital data acquisition (DAQ) solution for monitoring and controlling lithography semiconductor manufacturing subsystems to meet the production challenges faced by wafer fabricators and integrated device manufacturers.

Application background

The continued miniaturization of semiconductors is driving performance gains in everything from smartphones to supercomputers, and the processing requirements of generative artificial intelligence (GenAI), quantum computing, IoT,

and edge computing. Advanced processes and innovative control systems are required to meet the ever-decreasing size requirements of semiconductors with circuits as narrow as one-ten-thousandth the width of a human hair.

Lithography is a cornerstone technology in semiconductor manufacturing that enables the precise patterning of features on silicon and other substrate wafers to create ICs. It utilizes photomasks and powerful, extremely accurate light beams or radiation to transfer the details of a chip's design pattern onto wafers, which are coated with photoresist material. The photoresist reacts to the light, and the wafer is treated with chemicals to etch the circuit pathways in the wafer substrate. Multiple photomasks are utilized in a layering process.

The highly specialized and extremely complex lithography semiconductor manufacturing systems are produced by a very small number of companies able to undertake the technical challenges and fund the expensive R&D needed for continued innovation in this field.

ASML is the industry leader, dominating the advanced lithography market with its exclusive, cutting-edge extreme ultraviolet (EUV) systems, which are essential for producing the most advanced chips. Costing up to

hundreds of millions of dollars, the company's most advanced systems now enable the production of chips with feature sizes smaller than 2 nm, providing more transistors per chip and smaller spacing between transistors. It also supplies deep ultraviolet (DUV) systems that utilize longer wavelengths suitable for more cost-effective production of mid-range and legacy layers on chips manufactured at 14 nm, 28 nm, and larger nodes.

Other lithography semiconductor manufacturing systems are produced by Canon and Nikon, which focus on DUV lithography and legacy technologies for manufacturing less advanced nodes used in MEMS, power semiconductors, and industrial applications.

Achieving extreme precision

Lithography processes require extreme precision to achieve sub-micron scale patterns. Sensors and actuators are critical to maintain precision and yield, enabling continued technological advances in the development of smaller, more potent, and energy-efficient semiconductors.

Sensors play a pivotal role in actuator control, providing real-time feedback, error correction, and environmental compensation:

- Position sensors measure the exact position of wafers, photomasks, and lenses
- Vibration sensors detect and compensate for vibrations that can disturb alignment
- Environmental sensors monitor temperature, humidity, and air quality to minimize environmental influences on precision
- Force and strain sensors ensure actuators apply the correct forces during alignment and positioning

Sensors provide the essential real-time data for closed-loop feedback to adjust actuators dynamically, ensuring alignment and pattern accuracy. They detect deviations in real time to prevent defects in patterned wafers and perfect alignment of the photomask and wafer, which is crucial for multi-layer chip designs. They are also critical for minimizing delays caused by misalignments or rework.

Interaction of sensors and actuators

DUV and EUV lithography systems both rely on tens of thousands of sensors to achieve the precision and reliability essential for efficient, high-yield semiconductor manufacturing. As equipment

manufacturers aim to achieve picometer scale for next-generation lithography, the role of sensors and actuators in ensuring precision and reliability becomes ever more critical. The seamless interaction and management of those components are central to the success of lithography systems.

Managing these sensors requires real-time data processing and advanced control systems. Interaction between sensors and actuators in lithography systems must be meticulously orchestrated to attain the precision and reliability demanded by semiconductor manufacturers and their customers. The intricate processes hinge on real-time feedback mechanisms, sophisticated control algorithms, and seamless integration across intricate subsystems.

Sensors continuously monitor parameters such as position, temperature, pressure, and vibration. Any deviation from desired parameters must be corrected in real time. Actuators are directed to respond with micro or nano-scale adjustments to position the wafer or mask, and fine-tune the optical focus or light source alignment.

In wafer stage positioning, sensors track movements with sub-nanometer precision. Actuators, such as linear motors

or piezoelectric elements, dynamically adjust the stage's position to maintain accurate alignment with the photomask. Optical alignment sensors monitor the light path, and actuators adjust mirrors or lenses to ensure focus and pattern accuracy.

Centralized control

Centralized control units monitor and process data from thousands of sensors and send commands to actuators. These systems utilize high-speed processors and sophisticated algorithms to manage interactions seamlessly, ensuring synchronization across multiple subsystems. Achieving nanometer-level accuracy requires minimal delays in data processing and actuator response.

Sensors and actuators are connected via high-speed, low-latency communication protocols like EtherCAT, Ethernet, or proprietary interfaces. These networks facilitate rapid data exchange and coordination between components.

Drift in sensor readings or actuator performance is detected through monitoring and compensated using adaptive control algorithms. Machine learning algorithms analyze historical data to predict potential deviations

or equipment wear, enabling predictive maintenance and optimized actuator performance.

As semiconductor nodes continue to shrink, the role of sensor and actuator integration is increasingly critical. Interferometers measure the wafer stage position with nanometer precision, while actuators dynamically adjust the stage position based on feedback from alignment and vibration sensors. Optical sensors monitor light focus and intensity, and piezoelectric actuators adjust lenses or mirrors to maintain focus for accurate projection of circuit designs onto the wafer. Cameras or optical sensors are also utilized to detect particles or irregularities, with actuators being prompted to reposition the wafer or mask to avoid defects, or initiate automated cleaning procedures.



Figure 1: ADI's ADAQ7768-1 μ Module data acquisition system. (Image source: Analog Devices, Inc.)

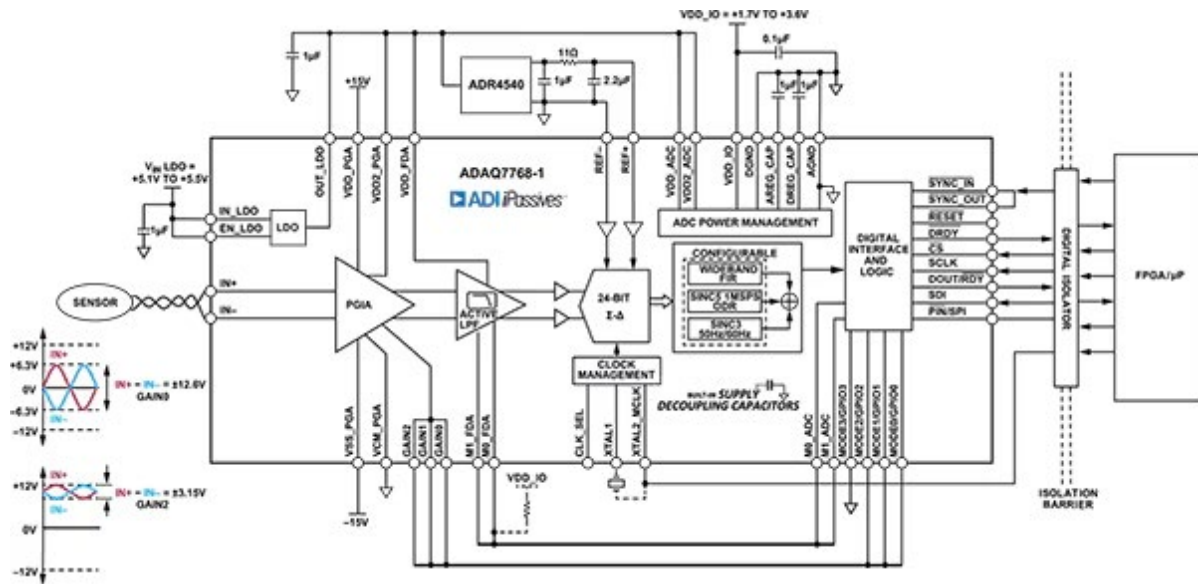


Figure 2: A block diagram of the ADAQ7768-1 μ Module. (Image source: Analog Devices, Inc.)

Signal chain performance

In each lithography semiconductor manufacturing system, the performance of each sensor is critical. ADI's [ADAQ7768-1](#) (Figure 1) is a DAQ system based on the company's μ Module technologies that is designed to simplify and enhance the performance of precision measurement and control systems. The single system-in-package (SiP) solution incorporates high input impedance amplification, anti-aliasing, signal conditioning, analog-to-digital (A/D) conversion, and configurable digital filtering blocks.

By integrating passive components such as resistors and capacitors and active components such as op-amps, references, low dropout regulators (LDOs), and A/D conversion, μ Modules guarantee the performance of a complete signal chain over temperature and power supply variations. This ensures precise and repeatable high-performance signal chains for acquiring signals from pressure, temperature, and vibration sensors.

The ADAQ7768-1 integrates multiple components into a single μ Module, as shown in the Figure 2 block diagram. These include a 24-bit precision analog-to-digital converter (ADC),

signal conditioning components such as amplifiers and filters, and power management and reference circuitry.

The 24-bit ADC enables precise measurements of delicate parameters such as vibration levels in wafer stages, thermal variations in optical assemblies, and sub-nanometer positioning errors.

Multiple sensors—such as pressure, temperature, and vibration—can be wired to the ADAQ7768-1's analog front end (AFE), which includes multiple active and passive components. Multiple modules can be used in parallel to manage data from a large array of sensors.

such as those monitoring wafer stage alignment or environmental conditions.

Power supply noise can directly impact the precision and reliability of lithography system measurements, but the ADAQ7768-1 was designed to operate with a single power supply, simplifying system design and reducing the need for additional external power management circuits.

The power management design minimizes power supply ripple and noise, which is critical for maintaining the high accuracy of the integrated low noise 24-bit ADC and the signal conditioning chain.

The ADAQ7768-1 is designed to operate using a single regulated 5.3 V input, with minor variation of input voltage range between 5.1 V and 5.5 V. The module includes internal LDOs to provide clean and stable power to its various internal subsystems.

The ADAQ7768-1 reduces design complexity by eliminating the need for designers to source and calibrate individual signal chain components, helping to streamline prototyping and testing phases, thereby shortening the time-to-market.

Product designers can utilize ADI's [EVAL-ADAQ7768-1](#) evaluation board (Figure 3) to

simplify prototyping, accelerate development, and help validate precision data acquisition designs that integrate the ADAQ7768-1 into their systems. This is critical in ensuring systems perform as expected in sub-nanometer positioning and alignment processes.

The evaluation board provides a fully functional platform to test the ADAQ7768-1 with pre-assembled signal chain components and offers plug-and-play operation with standard test equipment or microcontrollers. Designers can evaluate and optimize the performance of their designs, test under various environmental conditions test differing sensor types and signal sources to determine optimal input signal conditioning.

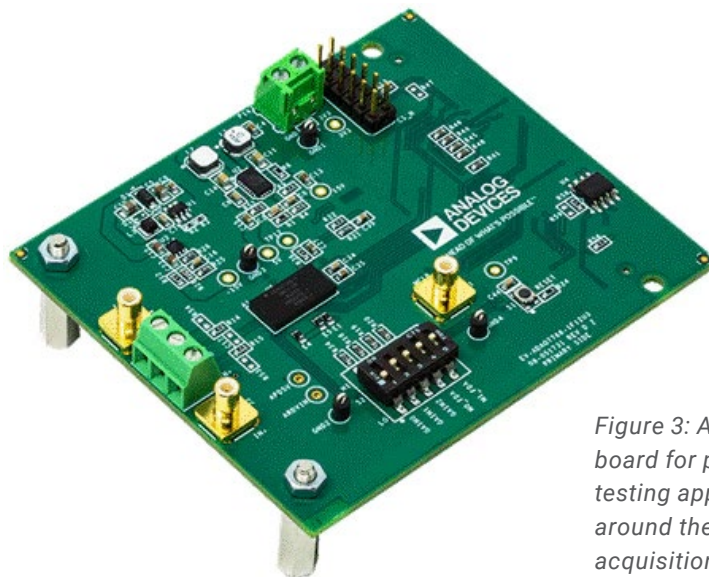


Figure 3: ADI's evaluation board for prototyping and testing applications built around the ADAQ7768-1 data acquisition solution. (Image source: Analog Devices, Inc.)

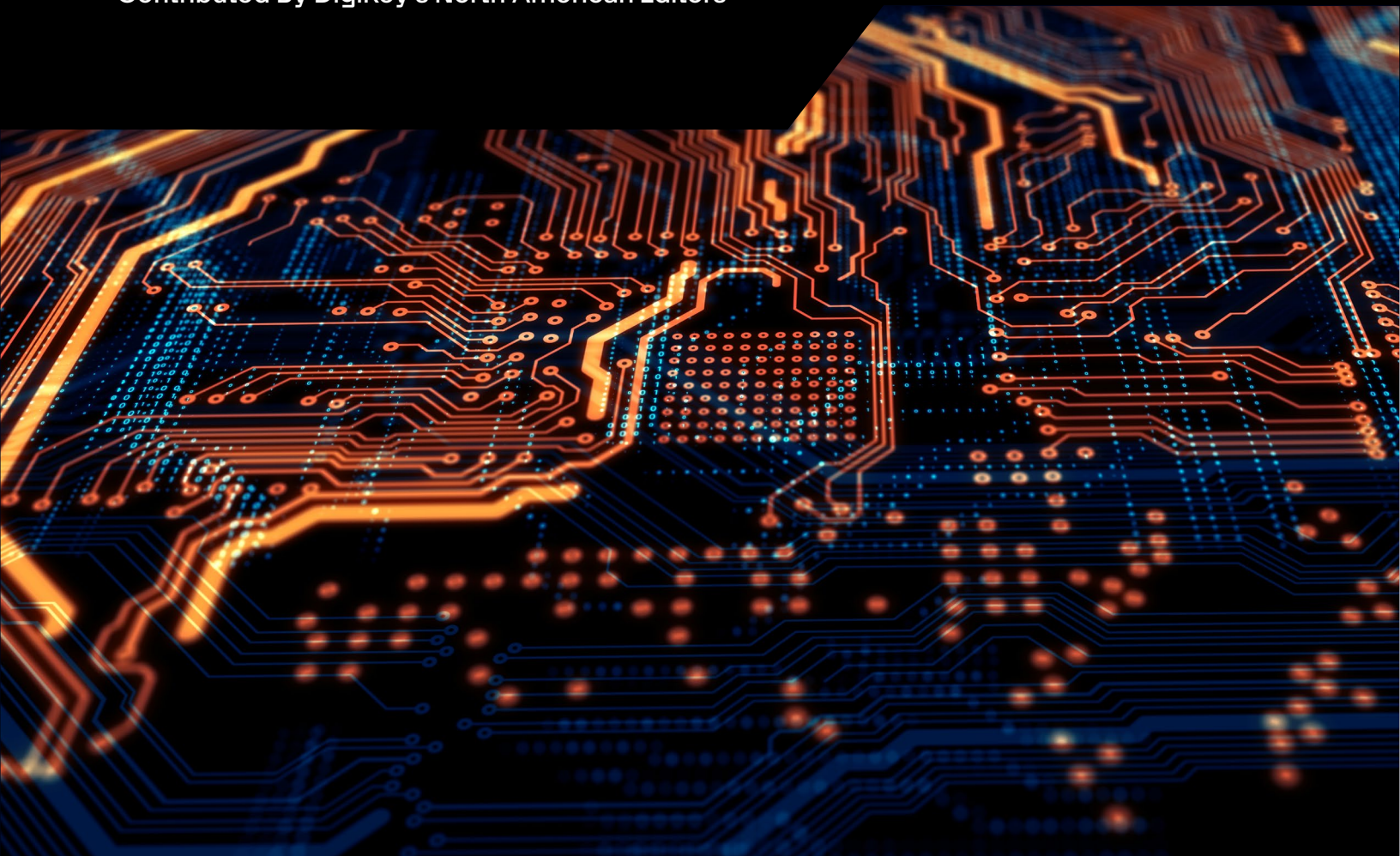
Conclusion

Advanced lithography systems, which rely on thousands of sensors for monitoring and control, are crucial for manufacturing smaller and more powerful semiconductors. Sensors play a pivotal role in actuator control, providing real-time feedback and ensuring precision and yield in semiconductor manufacturing. ADI's ADAQ7768-1 data acquisition system simplifies and enhances precision measurement and control systems, integrating signal conditioning, conversion, and processing blocks. Its compact size, high accuracy, and ease of use make it a valuable tool for developing next-generation lithography equipment that demands extreme precision and reliability.

Take advantage of I3C for faster, simpler, and more flexible IC-to-IC communication

By Art Pini

Contributed By DigiKey's North American Editors



Onboard serial interfaces for integrated circuit (IC)-to-IC communications are dominated by the Inter-Integrated Circuit (I²C) and the Serial Peripheral Interface (SPI), which have been available since the 1980s. These interfaces are widely used for connecting lower-speed sensors and ICs to microcontroller units (MCUs) for intra-board communication over short distances. However, as digital systems get faster, these interfaces, limited to typical data rates of 1 megabit per second (Mbit/s) for I²C and 10 Mbits/s for SPI, have become a limiting factor. Other limitations, including dedicated interrupt or chip enable lines, require additional signal connections, increasing the number of wires and complexity of the bus connections.

The Improved Inter-Integrated circuit (I3C) bus is intended to upgrade inter-IC communications. It offers higher data rates, greater flexibility, and a true two-wire interface with in-band interrupts (IBIs) instead of external ones.

This article discusses the characteristics of the I3C interface and why it might be a good upgrade from the I²C and SPI serial interfaces. Typical MCU, IC switch, and sensor devices will be used to show its application.

Embedded communications buses

Embedded serial interconnects like I²C and SPI have been employed for many years for intra-board communications. They are primarily used as communications buses

between sensors and user interface devices and their control processors. The number of sensors in typical systems has grown to ten to twenty in a phone and significantly more in vehicles. At the same time, communication requirements have become more challenging for designers as the demand increases for higher speed, lower power consumption, and fewer conductors. Designers must meet these demands while maintaining processor control via interrupts and enable lines (Figure 1).

Current technology implements the sensor and user control device interface using two-wire I²C or four-wire SPI interfaces. Interrupt, enable, and other control lines are separate from the clock and data lines, resulting in more lines per interface.

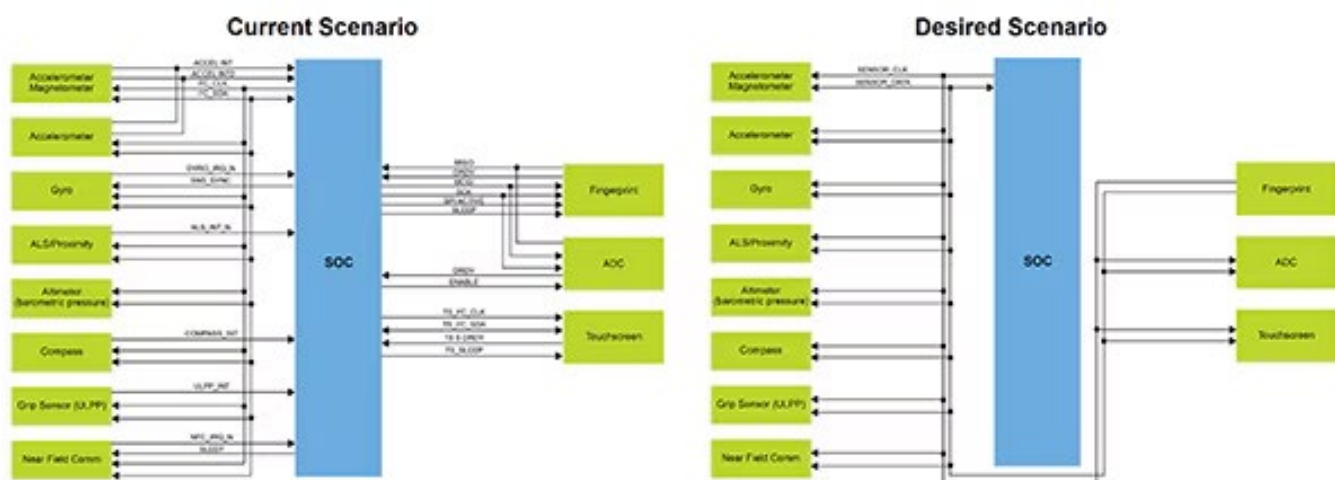


Figure 1: Embedded communications should support higher speeds, lower power, and a minimum wire count.
(Image source: [NXP Semiconductors](#))

Designers need a more forward-looking interface approach that eliminates these extra conductors from the interconnects and handles those operations in-band using only the clock and data lines. Additionally, the bus should be able to operate at higher speeds and with lower power losses.

I3C interface

I3C was developed by the Mobile Industry Processor Interface (MIPI) Alliance to address these requirements. The interface is available both as MIPI I3C to MIPI members, and as MIPI I3C Basic with reduced functionality to non-members. Like the legacy I²C

and SPI interfaces, the improved form is serial and is implemented using two wires to minimize pin counts and the number of signal paths between components. It has a data rate up to 12.5 Mbits/s with a 12.5 megahertz (MHz) clock using single data rate (SDR) mode. It operates at lower power levels and uses a simple yet flexible design architecture.

Notably, the I3C standard retains limited backward compatibility with the I²C system, allowing existing I²C devices to be connected to the I3C bus, while still allowing the bus to switch to higher data rates for communication between compliant I3C devices.

A comparison of the system configurations is shown in Figure 2.

The four-wire SPI interface can operate faster and supports full duplex communication. I²C communicates using half duplex over a two-wire bus consisting of a clock (SCL) and data (SDA) lines. Both require extra lines to support interrupts and other control functions such as chip select. I3C reduces the number of wires used in the interface to two, eliminating the separate interrupt, enable, and chip select lines used in I²C and SPI. This reduction in wire count is a significant advantage in a system requiring ten to twenty individual

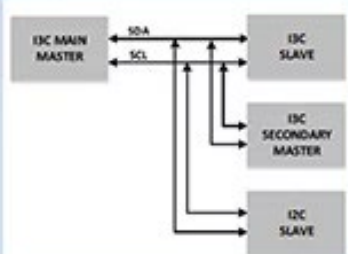
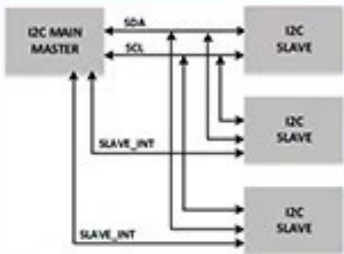
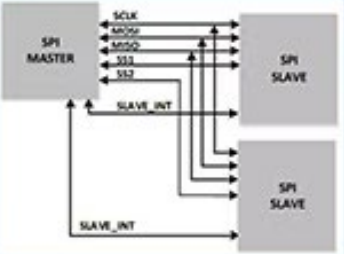
Parameter	MIPI I3C	I ² C	SPI
Overview			
# of lines	2-wire	2-wire (plus separate wires for each required interrupt signal)	4-wire (plus separate wires for each required interrupt signal)
Effective Data Bitrate	33.3 Mbps max at 12.5 MHz (Typ.: 10.6 Mbps at 12 MHz SDR)	3 Mbps max at 3.4 MHz (Hs) 0.8 Mbps max at 1 MHz (Fm+) 0.35 Mbps max at 400 KHz (Fm)	Approx. 60 Mbps max at 60 MHz for conventional implementations (Typically: 10 Mbps at 10 MHz)

Figure 2: Comparing the basic configurations of I3C, I²C, and SPI interfaces shows I3C's improved speed and simpler wiring. (Image source: NXP Semiconductors)

sensors tied to the processor, each with several secondary wires. Interrupts and other control lines are replaced by IBIs. In this method, a target sensor or device imposes its address into the I³C bus address header to notify the processor of an interrupt.

The difference in clock rates between I²C and I³C is significant. I²C is generally clocked at 100 kilohertz (kHz), 400 kHz, or 1 MHz, while I³C can be clocked at 12.5 MHz. Previously, SPI was used for clock rates higher than 1 MHz. The

design selection was between the clock rate and the number of wires. I³C has changed that by offering higher clock and data rates using a true two-wire topology.

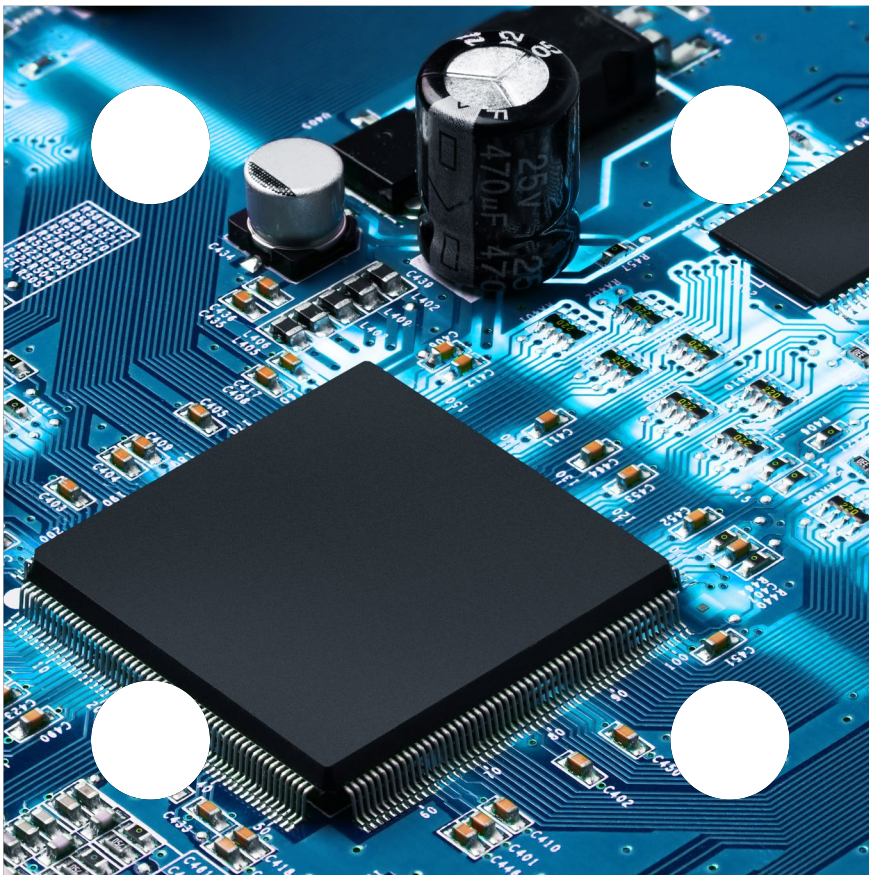
Push-pull outputs, which can switch faster than open-drain or collector drivers, are significant contributors to I³C's increased clock rate. To maintain compatibility with I²C devices, I³C can switch between open-drain and push-pull drivers depending on the bus state. The open-drain or collector design

is used during initial addressing or arbitration, where both I²C and I³C devices may be on the line simultaneously. I³C uses push-pull when communication is unidirectional, and there is no chance of an I²C device communicating simultaneously.

In addition to the standard SDR, I³C supports several optional high data rate (HDR) modes. These HDR modes operate with the same clock rate but transmit with a higher data density. The first of the HDR modes is HDR double data rate (HDR-DDR), where data is clocked on both edges of the clock signal, providing nearly two times the data rate. For a 12.5 MHz clock, the DDR mode achieves an effective data rate of 20 Mbits/s.

HDR ternary symbols have dual versions: HDR ternary symbol, pure (HDR-TSP) for I³C devices only, and HDR ternary symbol, legacy (HDR-TSL) for buses including both I²C and I³C devices. Ternary symbol modes achieve three data bits per clock using three-bit (ternary) symbols encoded on the SCL and SDA lines.

HDR bulk transport (HDR-BT) mode offers the highest data by supporting communications over quad, dual, or single SDA data lines. This results in eight, four, or two times the raw single data rate performance at the same clock rate.



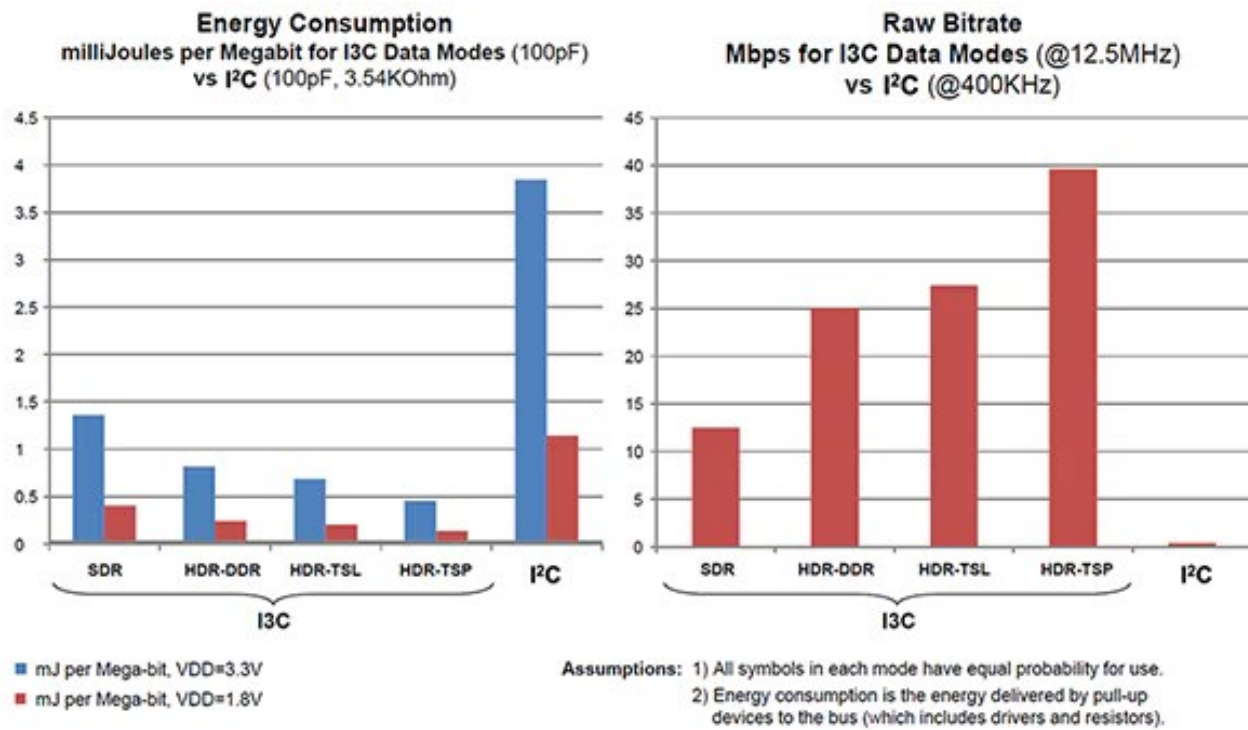


Figure 3: I3C offers improvements in data rate and power consumption compared with I²C.
(Image source: NXP Semiconductors)

These increases in the data transfer speed allow devices to be turned on for a shorter period, reducing the bus power duty cycle. This reduces power consumption compared with I²C (Figure 3). The change from open-collector drivers with external pull-up resistors to push-pull drivers further reduces power consumption, as the pull-up resistors require significant power to operate.

Addressing

I²C uses static addresses of either 7 or 10-bit length for each bus device. This has been changed in I3C to 7-bit dynamic addressing, where the bus master sets the device address during dynamic address assignment (DAA), and stores it in a device register. Static addressing, as in the case of an I²C peripheral, can still be used in I3C.

Due to dynamic addressing, device addresses can be changed later. This supports hot joining, which allows a new device to be added to the bus while it operates. The new device, connected to the I3C bus, signals its presence to the I3C master by sending a hot join request. The master controller acknowledges the request and assigns an address to add the device to the bus.

IBIs

I3C is a true two-wire bus that uses IBIs instead of dedicated interrupt lines like I²C. IBIs are when a target device signals its availability to the master by pulling down the SDA line. The master then starts the clock on the SCL line, and the target device transmits its address onto the I3C bus to notify the controller of an interrupt.

Common command codes

Common Command Codes (CCC) are standardized commands that the controller can transmit as a general broadcast to all I3C devices simultaneously or to a specific target device. These commands are for items related to bus management. The format of the CCC protocol begins with the I3C broadcast address, which is recognized by all I3C devices on the bus. Any I²C device on the bus will not acknowledge the request as it is a reserved I²C address.

Each command includes an 8-bit descriptor ID field and may be followed by a command payload. A command sent to a specific device passes the device address in the first byte of the payload. There are over forty CCC commands, including:

- Enter Dynamic Address Assignment (ENTDAA)
- Set New Dynamic Address Assignment (SETNEWDA)
- Enable Events (ENEC)/Disable Events (DISEC)
- Reset Dynamic Address Assignment (RSTDAA)
- Enter High Data Rate Mode (ENTHDRx)
- Get Device Characteristics Register (GETDCR)
- Vendors are allowed a dedicated range of CCC IDs to implement their own commands.

Error detection and recovery

Unlike I²C, I3C includes provisions for error detection and recovery. Six error and recovery methods for target devices are mandated, and another is optional. Additional error and recovery methods are also available specifically for master-side errors.

I3C supported components

As shown in Figure 2 (left), a basic I3C network comprises at least one master controller and one or more I3C targets or

slaves. The main master can be an MCU such as the NXP Semiconductors [LPC5534JHI48-00MP](#) (Figure 4). It is a 32-bit Arm® Cortex®-M33 MCU with 128 kilobytes (Kbytes) of SRAM and 256 Kbytes of Flash. Its Flexcomm interface supports eight different serial interfaces, including I3C.

The I3C bus allows the addition of secondary masters introduced to the bus as slaves. The I3C can have multiple masters, but only one can be the controller. Once enrolled, the secondary master can request the current master status, and if the current master accedes, its control is handed over to the requesting secondary master.

A typical I3C sensor is NXP's [P3T2030CUKAZ](#). This temperature sensor converts temperatures from -40°C to +125°C into a 12-bit digital value with an accuracy of ±2°C. It includes both an I²C and an I3C SDR mode serial interface.

A more sophisticated sensor is the [ICM-42605](#) three-axis microelectromechanical systems (MEMS) gyroscope and accelerometer from [TDK InvenSense](#). As a rate gyro, it measures spin rates from ±15.2 to ±2000 degrees per second (°/s). Its range as an accelerometer is ±2 to ±15 g. It detects motion, tilt, tap, or steps

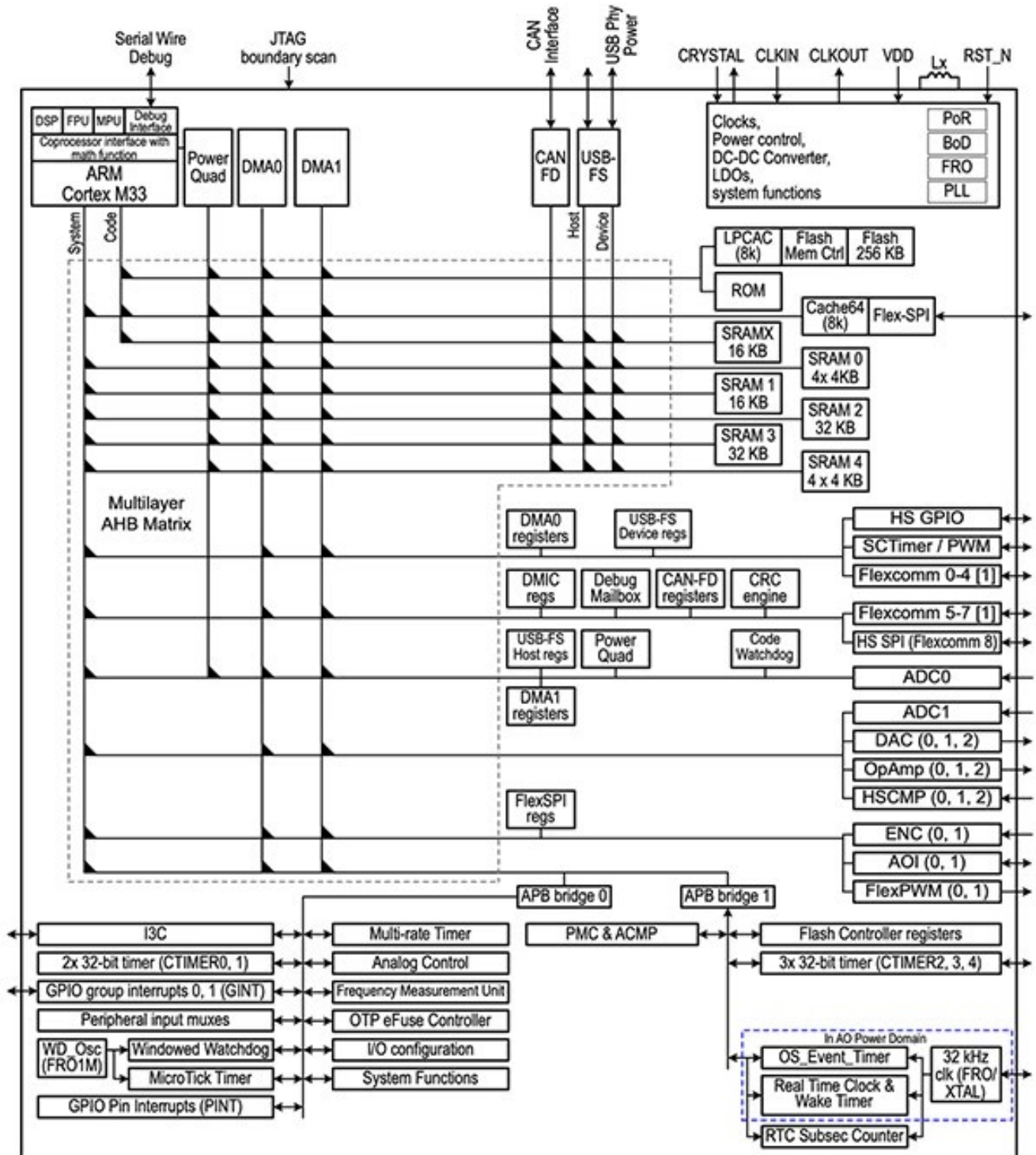


Figure 4: The LPC5534JHI48/00MP MCU includes an I3C interface and seven other serial interfaces.
(Image source: NXP Semiconductor)

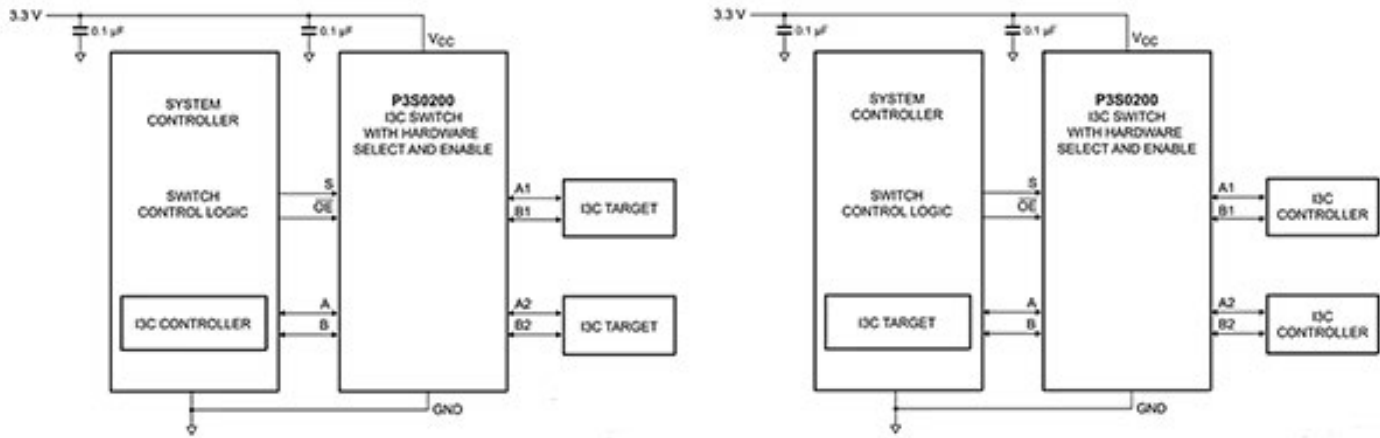


Figure 5: The P3S0200GMX I3C switch can be used to reconfigure an I3C bus by routing I3C bus signals between an I3C controller and multiple sets of target devices, or between a single target and multiple I3C controllers. (Image source: NXP Semiconductors)

(pedometer). As an I3C sensor, it operates at 12.5 MHz in SDR mode and 25 MHz in DDR mode.

ICs such as the NXP

P3S0200GMX I3C switch can reconfigure the I3C bus by routing I3C bus signals between an I3C controller and multiple sets of target devices, or between a single target and multiple I3C controllers as determined by an external MCU (Figure 5).

Switching between two targets might be required if both targets have the same address and cannot reside on the same bus. Alternatively, a single target

might have to be shared between two processes, requiring a switch between the two I3C controllers.

Conclusion

I3C is a serial interface that extends the I²C bus by increasing its data rate, reducing the number of wires, and adding flexibility to the bus control. It is an enhancement that extends the usefulness of legacy I²C and SPI interfaces.

Arduino sample code for SPI absolute encoders

By Damon Tarry, Design Applications Engineer, Same Sky

This Arduino sample code tutorial aims to give users a solid starting point for configuring and reading data from [Same Sky's AMT22 absolute encoders](#) with Serial Peripheral Interface (SPI) communication. The tutorial will provide what hardware and software is needed, key setup requirements, and sample code packages and instructions for both single-turn and multi-turn output options. Here is a list of what is required to get started:

- [Arduino board](#)
- [AMT22 encoder](#)
- [AMT-06C-1-036 cable](#), or similar cable with proper connector
- [Arduino IDE](#)
- [Download AMT22 Single-Turn Sample Code](#)

- [Download AMT22 Multi-Turn Sample Code](#)

AMT22 absolute encoder overview

Same Sky's (formerly CUI Devices) AMT22 is an absolute encoder offered in either 12-bit or 14-bit resolution, meaning it provides a precise number of unique positions per revolution. For the 12-bit variant, this translates to 4,096 distinct positions, while the 14-bit model features 16,384 positions per revolution. Regardless of how many times the device is rotated, it continuously reports its absolute position, giving users accurate feedback on the device's exact angle.

This encoder is available in both single-turn and [multi-turn models](#). The single-turn variant

measures position within a single 360-degree rotation, while the multi-turn version tracks not only the position within a rotation but also the total number of complete rotations. Additionally, the single-turn variants feature a programmable zero point, enabling users to define a custom reference for the encoder's origin.

Getting started

Ensure that the device is in RUN mode by adjusting the switch located on the back of the encoder to the appropriate position (Figure 1). Now mount the AMT22 encoder to a motor or assembly using the [AMT mounting instructions](#) to ensure proper installation. The AMT22 supports 9 different shaft sizes ranging from 2 mm to 8 mm.

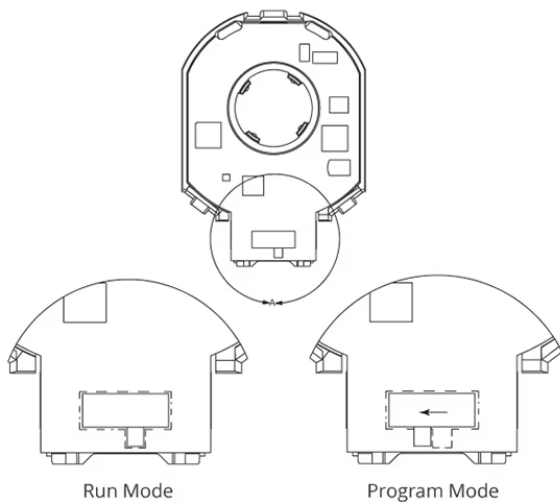
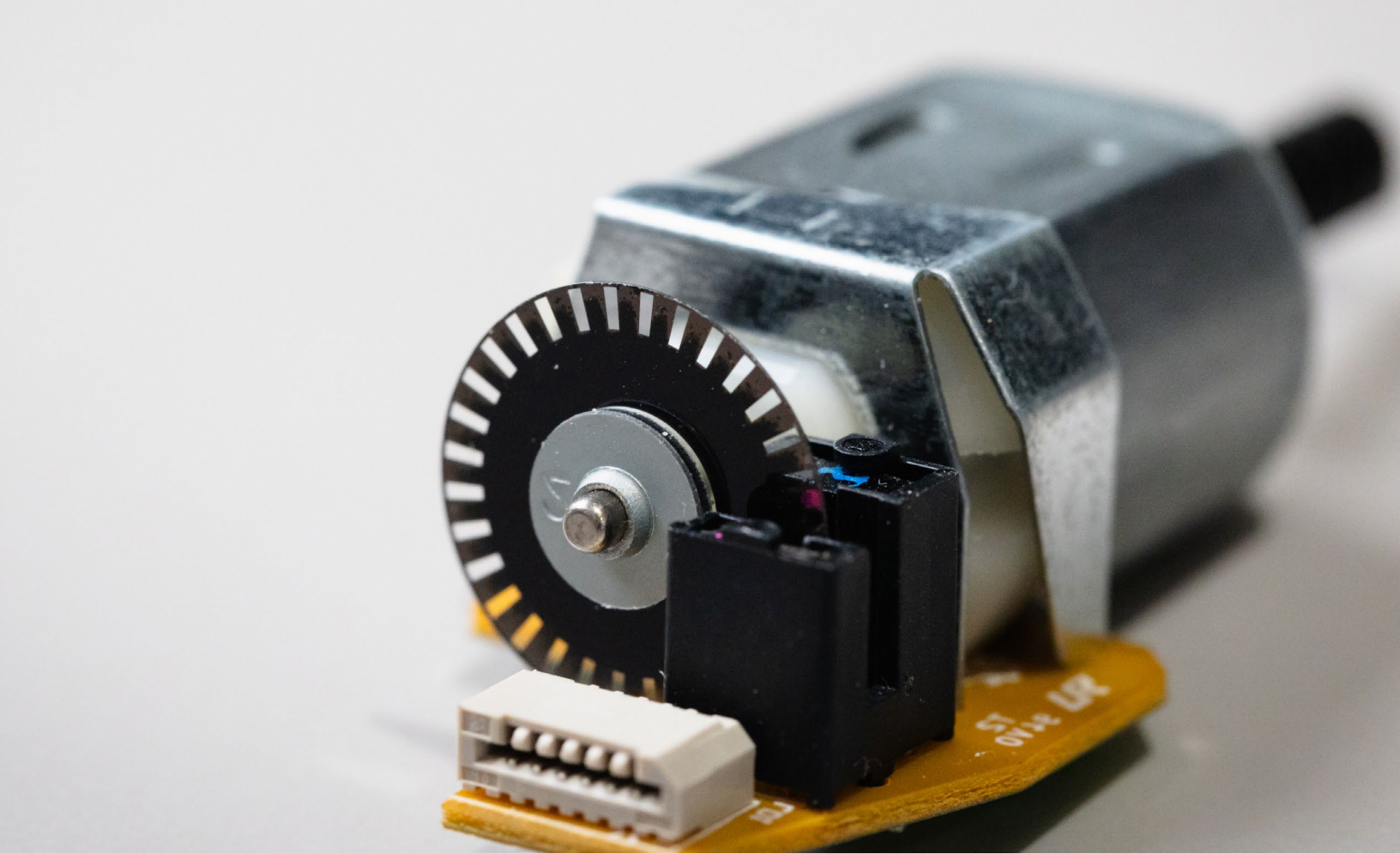


Figure 1: Flip the switch on the back of the AMT22 encoder to RUN mode. (Image source: Same Sky)

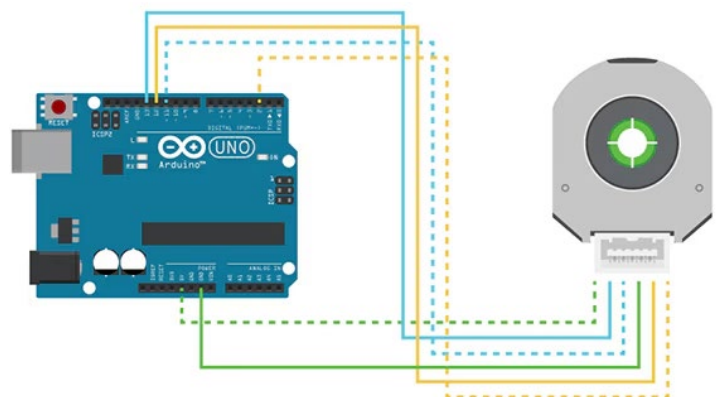


Figure 2: Arduino Uno wiring connections with the AMT22 encoder. (Image source: Same Sky)

The connections outlined in Figure 2 and Table 1 are specifically for the [Arduino Uno board](#), but the provided code should be

compatible with most Arduino boards. However, keep in mind that pin configurations may differ across various Arduino models.

For precise connection details on other boards, it's recommended to refer to the corresponding Arduino documentation.

PROPERTY	ENCODER PIN NUMBER	ARDUINO UNO PIN	AMT-DBC-1-036
+5 V	1	5 V	White/green
SCLK	2	13	Blue/white
MOSI	3	11	White/blue
GND	4	GND	Green/white
MISO	5	12	Orange/white
CS	6	2	White/orange

Table 1: Arduino Uno wiring connections further defined. (Image source: Same Sky)

The AMT22 encoder starts transmitting its absolute position data immediately when the SPI communication begins, eliminating the need for a traditional command-response structure. During the first byte of the SPI transfer, the host sends 0x00, and the AMT22 responds simultaneously with valid position data.

If the host needs to issue a command (Table 2), such as a zero-setting command, it will be sent in the second byte of the transmission. This is referred to as an extended command. For detailed technical specifics, refer to the [AMT22 datasheet](#).

Code tutorial – includes and defines

Since the Arduino's SPI bus is being used to interface with the AMT22 encoder, the SPI

COMMAND	BYTE	NOTES
Get Position	0x00 0x00	
Set Zero	0x00 0x70	Single-turn only
Get Turns	0x00 0xA0	Multi-turn only

Table 2: AMT22 commands defined. (Image source: Same Sky)

library needs to be included in the code. To send the position data from the Arduino to the computer, the built-in USB-serial connection within the Arduino IDE is utilized, configured at a baud rate of 115200.

In addition, the commands used by the AMT22 need to be defined. Since the encoder doesn't process the content of the first byte, a NOP (no-operation) is assigned to simplify the communication process (Listing 1).

```

/* Include the SPI library for the arduino boards */
#include <SPI.h>

/* Serial rates for UART */
#define BAUDRATE    115200

/* SPI commands */
#define AMT22_NOP    0x00
#define AMT22_ZERO   0x70
#define AMT22_TURNS  0xA0

```

Listing 1: Setting up the SPI interface.

Initialization

In the `setup()` function (Listing 2), begin by initializing all required SPI pins and configuring the serial interfaces for communication.

The serial port should be initialized to allow data transmission to the host computer. This is done by

passing the defined `BAUDRATE` into the `Serial.begin()` function.

Before enabling SPI, ensure the chip select (CS) line is set to the appropriate state to prepare the encoder for communication.

Select a clock rate for the SPI bus to communicate with the AMT22.

For prototyping purposes, a clock rate of 500 kHz is suitable, although the AMT22 supports rates up to 2 MHz. Achieving 500 kHz can be done using the `SPI_CLOCK_DIV32` setting. Given the Arduino Uno's 16 MHz clock, this division results in a 500 kHz SPI clock rate. For more details on SPI clock configuration, consult Arduino documentation.

After configuring everything, the SPI bus can be initialized using `SPI.begin()`, which will set up the three dedicated SPI pins: MISO, MOSI, and SCLK, preparing the system for communication with the encoder.

```
void setup()
{
    uint8_t cs_pin = 2;

    //Set the modes for the SPI CS
    pinMode(cs_pin, OUTPUT);
    //Get the CS line high which is the default inactive state
    digitalWrite(cs_pin, HIGH);

    //Initialize the UART serial connection for debugging
    Serial.begin(BAUDRATE);

    //set the clockrate. Uno clock rate is 16Mhz, divider of 32 gives 500 kHz.
    //500 kHz is a good speed for our test environment
    //SPI.setClockDivider(SPI_CLOCK_DIV2); // 8 MHz
    //SPI.setClockDivider(SPI_CLOCK_DIV4); // 4 MHz
    //SPI.setClockDivider(SPI_CLOCK_DIV8); // 2 MHz
    //SPI.setClockDivider(SPI_CLOCK_DIV16); // 1 MHz
    SPI.setClockDivider(SPI_CLOCK_DIV32); // 500 kHz
    //SPI.setClockDivider(SPI_CLOCK_DIV64); // 250 kHz
    //SPI.setClockDivider(SPI_CLOCK_DIV128); // 125 kHz

    //start SPI bus
    SPI.begin();
}
```

Listing 2: The `setup()` function which initializes the all SPI pins.

SPI Communication

SPI communication with the AMT22 is handled through the Arduino's SPI library, while the chip select (CS) control is managed through the code using digital I/O pins. The `digitalWrite()` function is used to assert or deassert the CS line (Listing 3).

```
uint8_t cs_pin = 2;

//set the CS signal to low
digitalWrite(cs_pin, LOW);
delayMicroseconds(3);

//read the two bytes for position from the encoder, starting with the high byte
uint16_t encoderPosition = SPI.transfer(AMT22_NOP) << 8; //shift up 8 bits because this is the high byte
delayMicroseconds(3);
encoderPosition |= SPI.transfer(AMT22_NOP); //we do not need a specific command to get the encoder position, just no-op

//set the CS signal to high
digitalWrite(cs_pin, HIGH);
```

Listing 3: Setting up SPI communication.

The AMT22 expects two bytes of 0x00 to be sent, and it returns data immediately after receiving these bytes. Due to this fast response, certain minimum timing requirements must be followed, which are outlined in the AMT22 datasheet.

Regardless of whether the encoder is a 12-bit or 14-bit version, it always responds with two bytes (16 bits) of data. The upper two bits are check-bits, used to verify data integrity. For the 12-bit version, the lower two bits are both 0, and the returned value must be shifted right by 2 bits (or divided by 4) for proper use.

To obtain position data, the SPI.transfer() function is called, sending the AMT22_NOP command. The CS line remains low during this process. The AMT22 sends the high byte first, so the received byte is shifted left by 8 bits to align it in the upper half of a uint16_t variable.

This value is assigned to the encoderPosition variable in one operation. After a brief delay to meet the timing requirements, a second SPI.transfer() call is made to send another AMT22_NOP command. The result is OR'ed with the current value in encoderPosition, effectively combining the two received bytes into a single uint16_t variable. Finally, the CS line is released, completing the communication.

Checksum verification

After completing the SPI transfer, it is essential to validate the received data using a checksum (Listing 4).

To implement this validation, a function can be created based on the equation provided in the datasheet. The checksum is contained in the upper two bits of the received value, and it utilizes odd parity across the odd and even bits in the position response.

The function will perform the following steps:

1. Calculate the parity for the odd bits (bits 1, 3, 5, 7, 9, 11, 13)
2. Calculate the parity for the even bits (bits 0, 2, 4, 6, 8, 10, 12, 14)
3. Compare the calculated parities against the values indicated by the checksum bits

The function will return true if the checksum is valid, indicating that the data integrity is confirmed. If the checksum is invalid, the function will return false, signaling a potential error in the received data.

Data formatting

If the checksum validation confirms the integrity of the data, the next step is to update the encoderPosition variable by removing the upper two bits (Listing 5). This can be achieved by applying a bitwise

```
/*
 * Using the equation on the datasheet we can calculate the checksums and then make sure they match what the encoder sent.
 */
bool verifyChecksumSPI(uint16_t message)
{
    //checksum is invert of XOR of bits, so start with 0b11, so things end up inverted
    uint16_t checksum = 0x3;
    for(int i = 0; i < 14; i += 2)
    {
        checksum ^= (message >> i) & 0x3;
    }
    return checksum == (message >> 14);
}
```

Listing 4: Validating the checksum.

AND operation with 0x3FFF (or 0b0011111111111111), which effectively retains all 14 lower bits of the position data.

Additionally, it is necessary to account for the encoder's resolution—whether it is 12-bit or 14-bit. If the resolution is 12 bits, the encoderPosition value must be shifted 2 bits to the right to adjust for the lower resolution. This ensures that the position data is accurately represented

in the encoderPosition variable, reflecting the actual position of the encoder based on its specified resolution.

Set zero position (single-turn only)

Certain variants of the AMT22 encoder offer a programmable zero position feature. To set this zero position, a specific two-byte command sequence must be sent.

The process involves sending the AMT22_NOP command first, followed by a brief wait to meet the minimum timing requirements specified by the AMT22. After this wait, the AMT22_ZERO command is sent while ensuring the chip select (CS) line is released. Once the encoder receives this command, it will perform a reset operation (Listing 6).

```
if (verifyChecksumSPI(encoderPosition)) //position was good
{
    encoderPosition &= 0x3FFF; //discard upper two checksum bits
    if (RESOLUTION == 12) encoderPosition = encoderPosition >> 2; //on a 12-bit encoder, the lower two bits will always be zero

    Serial.print(encoderPosition, DEC); //print the position in decimal format
    Serial.write('\n');
}
else //position is bad
{
    Serial.print("Encoder position error.\n");
}
```

Listing 5: Updating the encoderPosition.

```
/*
 * The AMT22 bus allows for extended commands. The first byte is 0x00 like a normal position transfer,
 * but the second byte is the command.
 * This function takes the pin number of the desired device as an input
 */
void setZeroSPI(uint8_t cs_pin)
{
    //set CS to low
    digitalWrite(cs_pin, LOW);
    delayMicroseconds(3);

    //send the first byte of the command
    SPI.transfer(AMT22_NOP);
    delayMicroseconds(3);

    //send the second byte of the command
    SPI.transfer(AMT22_ZERO);
    delayMicroseconds(3);

    //set CS to high
    digitalWrite(cs_pin, HIGH);

    delay(250); //250 millisecond delay to allow the encoder to reset
}
```

Listing 6: Setting the zero position of a single-turn AMT22 encoder.

```
uint8_t cs_pin = 2;

//set the CS signal to low
digitalWrite(cs_pin, LOW);
delayMicroseconds(3);

//read the two bytes for position from the encoder, starting with the high byte
uint16_t encoderPosition = SPI.transfer(AMT22_NOP) << 8; //shift up 8 bits because this is the high byte
delayMicroseconds(3);
encoderPosition |= SPI.transfer(AMT22_TURNS); //we send the turns command (0xA0) here, to tell the encoder to send us the turns count after the position

//wait 40us before reading the turns counter
delayMicroseconds(40);

//read the two bytes for turns from the encoder, starting with the high byte
uint16_t encoderTurns = SPI.transfer(AMT22_NOP) << 8; //shift up 8 bits because this is the high byte
delayMicroseconds(3);
encoderTurns |= SPI.transfer(AMT22_NOP);
delayMicroseconds(3);

//set the CS signal to high
digitalWrite(cs_pin, HIGH);
```

Listing 7: Reading the encoderPosition and the turns counter in a multi-turn AMT22 encoder.

To avoid communication with the encoder during this reset period, a delay of 250 ms is implemented, ensuring that no commands are sent to the encoder during its power-on time.

While it is possible for the code to set the zero position of the encoder at the beginning of operation, it is more common in typical applications to set the zero position only once during the initial configuration of the device for use within the system. This practice helps maintain the integrity of the encoder's position feedback throughout its operational lifespan.

Read turns counter (multi-turn only)

Certain variants of the AMT22 encoder support a multi-turn counter, allowing users to read both

the position and the turn count in a single data retrieval sequence.

If the position data received is invalid, the system should notify the user of the error. In contrast, if the position is valid, the program should report the position in decimal format (Listing 7). This capability enhances the encoder's functionality by providing comprehensive feedback on both the absolute position and

the number of complete turns, facilitating more accurate monitoring and control in applications requiring precise rotational data.

Running the code

With the code successfully created, it's time to upload it to the Arduino and establish communication with the AMT22 encoder.

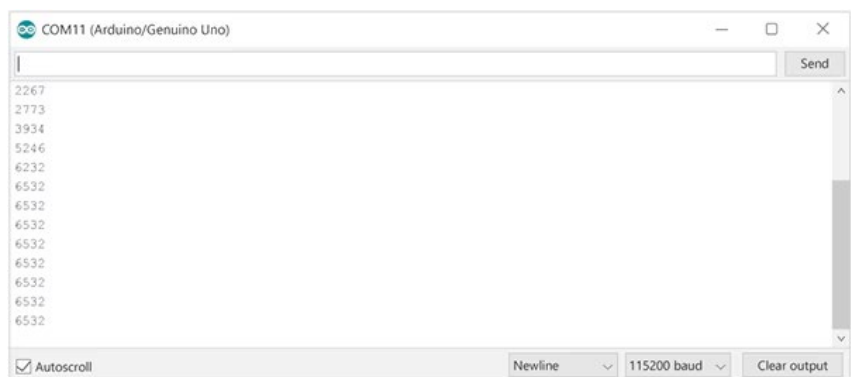


Figure 3: The reported position from the encoder, received by the Arduino (Image source: Same Sky)

To monitor the output, open the serial monitor in the Arduino IDE and ensure that the data rate is set to 115200 baud. This will allow users to observe the encoder's operation and view the reported position data in real time. Once the serial monitor is active, the encoder should start transmitting its position information, demonstrating its functionality within the system (Figure 3).

Multiple encoders

One significant advantage of using an SPI device is the ability to communicate with multiple

encoders on the same bus. To facilitate this, an additional digital I/O pin needs to be allocated for each encoder, allowing for individual chip select (CS) control.

In the example code (Listing 8), an array of CS pins is utilized to support an arbitrary number of encoders. This design allows for scalable communication, enabling the user to easily add more encoders as needed. By modifying the functions to accept the pin number corresponding to the desired device, the code can dynamically control which encoder is active on the SPI bus, ensuring

that each device can be accessed and operated independently.

The next step is to loop through each CS pin in the array and read the position from each connected encoder. This allows the system to activate each encoder by asserting its chip select line, performing the SPI transfer, and retrieving the position data. The code will sequentially select each encoder, execute the SPI communication, and release the CS line, ensuring that all connected devices are queried for their position information (Listing 9).

After the data transfer, a minimum wait time is required before releasing the chip select line. According to the datasheet, this minimum time is 3 microseconds. While this delay is typically observed naturally at slower data rates, it is good practice to implement it explicitly in the code to ensure proper operation and adherence to the timing specifications. This ensures reliable communication with the AMT22 encoder.

Conclusion

Users should now have a basic understanding of configuring and reading data from Same Sky's AMT22 absolute encoders. This article focused on the AMT22 absolute encoders. Same Sky also has a line of [AMT modular encoders](#) which offer a range of incremental, absolute, and commutation versions.

```
uint8_t cs_pins[] = {2}; //only one encoder connected, using pin 2 on arduino for CS
//uint8_t cs_pins[] = {2, 3}; //two encoders connected, using pins 2 & 3 on arduino for CS
```

Listing 8: Setting up an array for reading multiple encoders.

```
void loop()
{
  for(int encoder = 0; encoder < sizeof(cs_pins); ++encoder)
  {
    uint8_t cs_pin = cs_pins[encoder];

    //set the CS signal to low
    digitalWrite(cs_pin, LOW);
    delayMicroseconds(3);

    //read the two bytes for position from the encoder, starting with the high byte
    uint16_t encoderPosition = SPI.transfer(AMT22_NOP) << 8; //shift up 8 bits because this is the high byte
    delayMicroseconds(3);
    encoderPosition |= SPI.transfer(AMT22_NOP); //we do not need a specific command to get the encoder position, just no-op

    //set the CS signal to high
    digitalWrite(cs_pin, HIGH);

    if (verifyChecksumSPI(encoderPosition)) //position was good, print to serial stream
    {
      encoderPosition &= 0x3FFF; //discard upper two checksum bits
      if (RESOLUTION == 12) encoderPosition = encoderPosition >> 2; //on a 12-bit encoder, the lower two bits will always be zero

      Serial.print("Encoder #");
      Serial.print(encoder, DEC);
      Serial.print(" position: ");
      Serial.print(encoderPosition, DEC); //print the position in decimal format
      Serial.write('\n');
    }
    else //position is bad, let the user know how many times we tried
    {
      Serial.print("Encoder #");
      Serial.print(encoder, DEC);
      Serial.print(" position error.\n");
    }
  }

  //For the purpose of this demo we don't need the position returned that quickly so let's wait a half second between reads
  //delay() is in milliseconds
  delay(500);
}
```

Listing 9: Reading the encoderPosition variable from multiple encoders.

Learn the fundamentals of signal integrity

By Cece Chen

Contributed By DigiKey's North American Editors



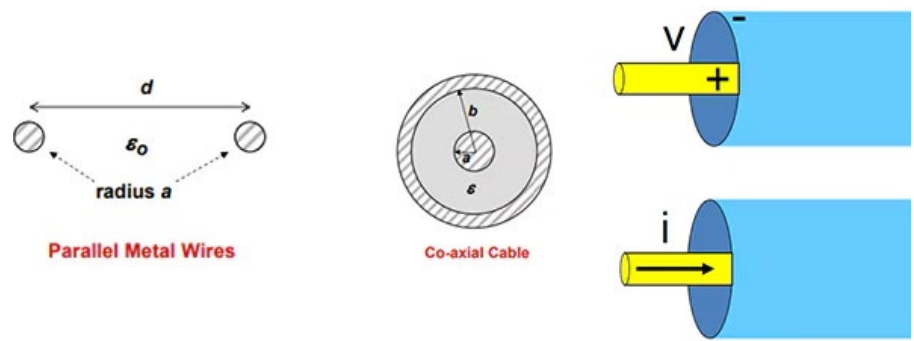


Figure 1: Transmission lines consist of conductors separated by a dielectric. The conductors can be parallel or concentric. (Image source: Amphenol)

The rise of high-performance data centers to support artificial intelligence (AI) makes signal integrity (SI) critical so that massive amounts of data can be moved at ever higher rates. To ensure SI, designers must minimize reflections, noise, and crosstalk through attention to board layout and the use of appropriate conductors and connectors. They must also understand fundamental principles such as transmission lines, impedance, return loss, and resonance.

This article presents some of the terms used in the discussion of SI and what designers need to consider. It then introduces exemplary cable and connector solutions from [Amphenol](#) to show how they can ensure design success.

Transmission lines

A transmission line consists of two (or sometimes three) conductors with non-zero length separated by a dielectric (Figure 1). Conductors carry electrical signals between circuit elements with minimal loss or distortion. Common conductors are metals such as copper, which have high electrical conductivity, excellent transmission, and low power losses at a relatively low cost. Gold is an excellent conductor, but due to its high cost, its use is restricted to applications requiring high corrosion resistance, like connector pins and sockets. Other metals and alloys have been developed for specific applications or material characteristics.

Dielectrics are nonconducting materials that separate conductors by insulating the area around their conducting geometries. The properties of the dielectrics impact how signals travel over the adjacent conductors.

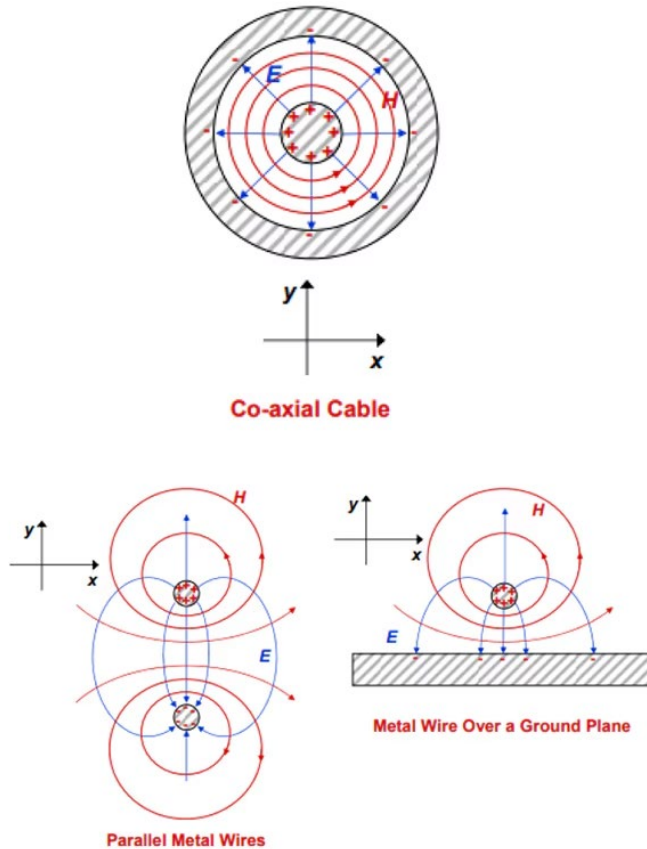
The dielectric constant (Dk) and dissipation factor (Df) are significant characteristics of dielectrics that impact transmission lines. The Dk determines the signal propagation speed on the line. For example, a material with a lower Dk has a higher propagation velocity. The Df represents the energy loss within the material as the signal travels down the transmission line. A lower Df indicates less signal attenuation, especially at high frequencies.

Common dielectrics are air and various plastics. A typical printed circuit board (pc board) substrate is a dielectric called flame retardant 4 (FR-4), a composite of woven fiberglass cloth impregnated with flame-retardant epoxy resin.

Standard transmission line configurations are coaxial cable, twisted pair, pc board stripline, and pc board microstrip. The two conductors are identified as the signal and return paths. The voltage on a transmission line is measured between the conductors along the line, and the current is measured through either of the conductors.

In SI, a transmission line is a distributed electrical component that carries transverse electromagnetic (TEM) or quasi-TEM waves between two conductors. These waves

Figure 2: Transmission lines propagate energy along the line using alternating orthogonal electric and magnetic fields. (Image source: Amphenol)



contain alternating electric (E) and magnetic (H) fields that are perpendicular to the wave's direction of travel (Figure 2).

A changing electric field creates a changing magnetic field as an alternating series of transformations, propagating the TEM wave along the transmission line in a direction perpendicular to both fields.

Transmission line connections between circuit elements are configured as single-ended or differential connections (Figure 3).

A single-ended configuration uses a signal line and a ground line. The signals are not identical, and the configuration is considered an unbalanced propagation mode. A differential configuration uses two complementary signal lines and a ground line, generally run separately. Differential signals are an example of a balanced propagation mode because the signal of interest is the mathematical difference between the two signal elements.

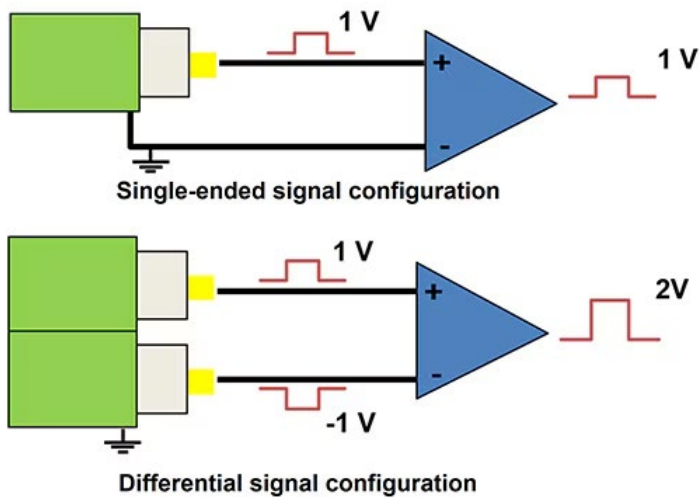


Figure 3: Transmission lines can be configured as either single-ended (unbalanced) using a signal and a return or ground conductor, or as differential (balanced) with two complementary signal conductors and a ground conductor. (Image source: Amphenol)

$$\text{reflection coefficient} = \frac{V_R}{V_I} = \frac{Z_L - Z_C}{Z_L + Z_C}$$

reflected voltage - V_R

incident voltage - V_I

load impedance - Z_L

transmission line impedance - Z_C

Figure 4: The reflection coefficient depends on the load and the transmission line's characteristic impedance. (Image source: Amphenol)

Transmission line impedance

Electrical impedance is a circuit's opposition to a current due to an applied alternating voltage, measured in ohms (Ω). Impedance is the complex ratio of the voltage

to the current at each point along the conductor.

Transmission lines must control their impedance to carry high-speed/high-bandwidth signals without degradation due to reflections. Their instantaneous impedance at each point in the

line is constant and referred to as the characteristic impedance. Trace width, spacing, length, and dielectric properties between the traces and the ground plane control the transmission line's impedance.

The characteristic impedance can be thought of as the resistance to energy transfer associated with wave propagation in a line much longer than the wavelength of the propagating signal.

Signal reflections

If a signal is propagated through a transmission line to a load with an impedance equal to the line's characteristic impedance, the signal is fully delivered to the load. If the load impedance differs from the line's characteristic impedance, then some of the energy incident on the load is reflected back toward the source.

The ratio of the amplitude of the reflected voltage, V_R , to the amplitude of the incident voltage, V_I , is the reflection coefficient (Figure 4). It depends on the load impedance (Z_L) and the transmission line's characteristic impedance (Z_C).

Reflections result from a signal transitioning across a boundary where the media have unmatched impedances (Figure 5). At each interface, the

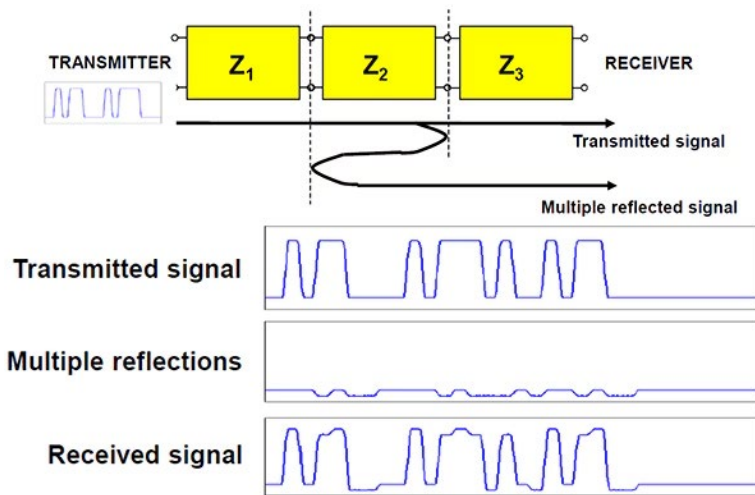


Figure 5: The transmitted signal is distorted by the reflected components summed with time delays proportional to the propagation delays of the reflection's path. (Image source: Amphenol)

Return Loss	Insertion Loss
$RL (dB) = 10 \log_{10} \frac{P_i}{P_r}$	$IL(dB) = 10 \log_{10} \frac{P_T}{P_R}$
where: P_i - Incident power P_r - Reflected power	where: P_T - Transmitted power P_R - Received power

Figure 6: The return loss measures reflected power in the frequency domain, while the insertion loss measures the power received at the load. (Image source: Art Pini)

reflection coefficient determines the amplitude and phase of the reflection. The signal at the receiver is the sum of the transmitted signal and the time-delayed reflections.

The junction of Z_2 and Z_3 reflects part of the incident signal back toward the transmitter while the bulk of the incident energy

continues to the receiver. The reflected signal encounters a mismatch in the reverse path and is partially reflected back toward the receiver. The edges of the signal are reflected with a polarity dependent on whether the impedance across the junction increases or decreases. The timing of the reflections depends on the physical distance between

the junctions. The receiver sees the sum of the transmitted signal and all the reflections.

Note that the received signal has nonuniform top and bottom levels due to the addition of the reflections. If the reflection amplitudes are high enough, errors can occur when reading the data. One of the critical goals of SI is the reduction of reflection anomalies.

Return loss and insertion loss

Transmission lines are characterized in both the frequency and time domains. Reflections are measured as return loss (RL) in units of decibels (dB) in the frequency domain (Figure 6). The portion of the incident power that fails to reach the load is characterized by the insertion loss (IL), also measured in dB. A lower insertion loss translates to a better connection.

The parameter describing insertion loss in bulk coaxial cable is attenuation per unit length specified as dB per foot (dB/ft.) or dB per meter (dB/m).

Noise

Noise is any undesired signal that appears on a transmission line. Reflections can be viewed

as a type of noise that can corrupt the received signal. Noise on a non-transmitting line can be received as a false signal.

Noise can come from several sources, such as thermal noise, external radiation impinging on a transmission line, and noise from another line within the same device (crosstalk). Energy from these sources adds to the signals on a transmission line. Noise is characterized by the signal-to-noise ratio (SNR), which is the ratio of signal power to noise power on a transmission line. The higher the signal-to-noise ratio, the better the signal quality.

Crosstalk

Crosstalk is a subcategory of unwanted noise that appears on a transmission line due to interactions with electromagnetic (EM) fields originating from adjacent lines without direct contact. Crosstalk is caused by line-to-line capacitive or line-to-line inductive coupling between an aggressor (carrier) and a victim (receiver) line (Figure 7).

Crosstalk is labeled according to where the victim experiences the coupled noise. Near-end crosstalk (NEXT) appears on the transmitter side of a transmission line or device under test (DUT),

Figure 7: Crosstalk can be caused by capacitive coupling of a voltage change or inductive coupling of a current change from the aggressor to the victim transmission line. (Image source: Amphenol)

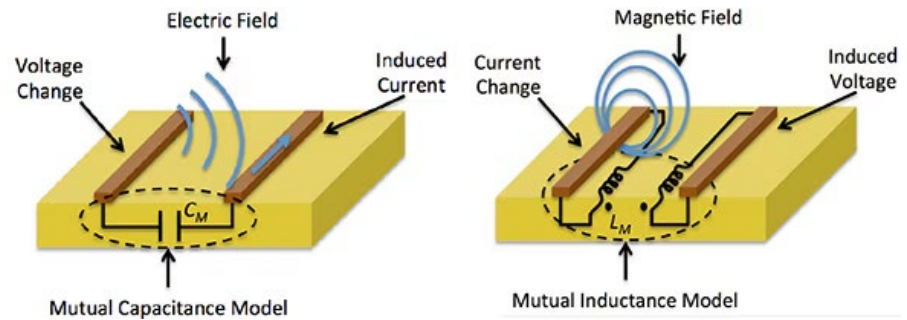
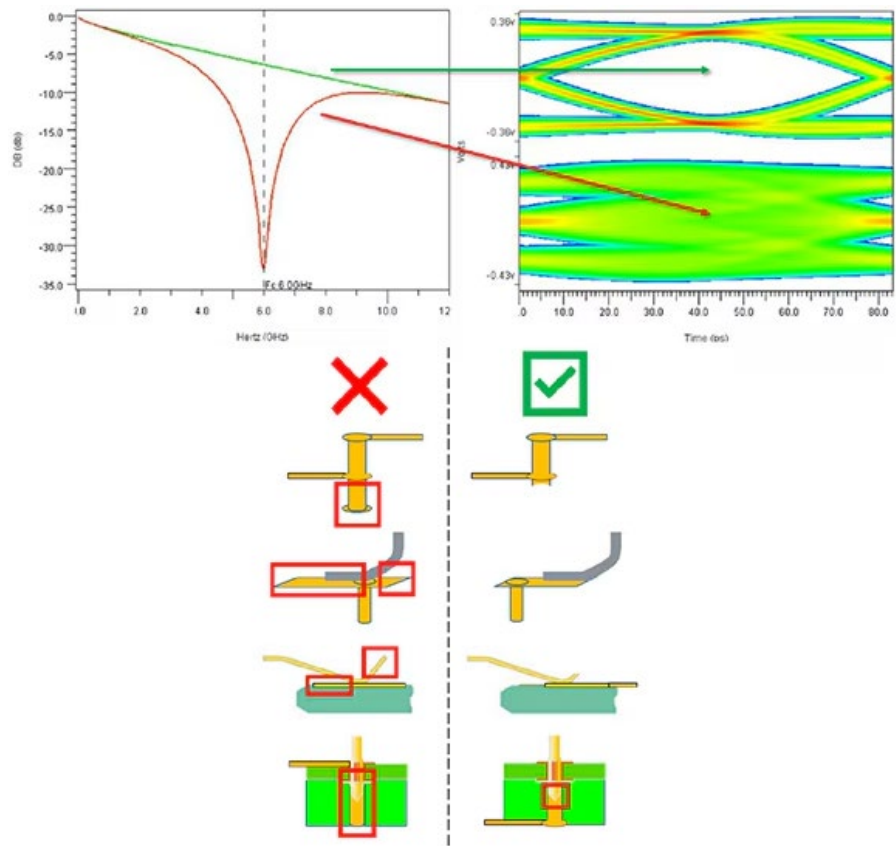


Figure 8: Shown are examples of resonance effects due to transmission line stubs of several kinds with two different lengths on a 12 Gbps channel. (Image source: Amphenol)



while far-end crosstalk (FEXT) appears on the receiver side.

Crosstalk can be reduced by increasing the distance between adjacent transmission lines, decreasing the path length, using differential lines that cancel noise common to both lines, keeping traces on adjacent pc board layers perpendicular, and incorporating integral grounding and electromagnetic interference (EMI) shielding.

Resonance

Resonance occurs when a signal's path is a multiple of a quarter of the signal's wavelength. At such points, the reflected signal overlaps the incident wave and either amplifies or attenuates the transmitted signal. The frequencies corresponding to these wavelengths are called resonances.

Resonances can cause noise or distort signals, and arise due to unterminated lengths of transmission lines, called stubs, in the signal path or non-ideal ground returns. Figure 8 shows resonance effects due to stubs of several kinds with two different lengths on a 12 gigabit per second (Gbps) channel.

The stubs highlighted with red boxes have a length of 0.25 inches (in.), resulting in a resonant frequency of about 6 gigahertz

(GHz). The three short stubs under the green checked box have a length of 0.025 in. Their resonant frequency is ten times higher or 60 GHz. Both spectral responses are shown in the spectrum analyzer plot in the upper left. The red spectrum is the response of the 0.25 in. stub, while the green trace is that of the 0.025 in. stub; the 0.25 in. stub shows a "suck out" response centered at 6 GHz with a very low amplitude.

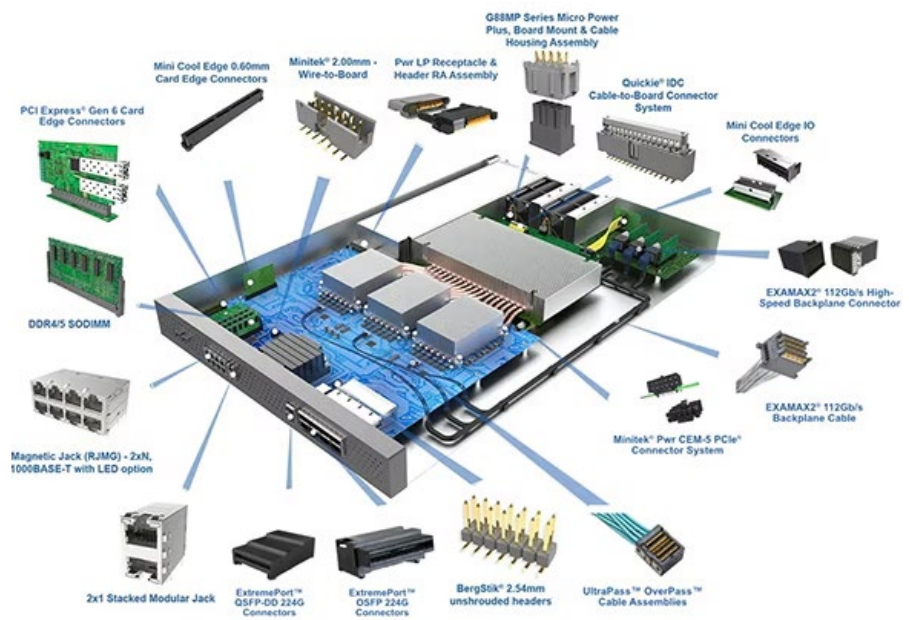
The eye diagram in the upper right corner overlaps multiple-bit sequences of 011, 001, 100, and 110 to produce a graphical SI measurement. As long as the eye remains open, the transmission is

successful. Vertical eye closures are due to noise, reflections, and crosstalk. Horizontal eye closures are related to timing issues like jitter. The 6 GHz resonance results in the collapsed eye due to the loss of signal amplitude.

SI in specifications for interconnection components

Interconnection components that support AI processors in data centers include coaxial and twisted pair cables, connectors, and pc boards (Figure 9). These components are usually specified in terms of characteristic

Figure 5: The transmitted signal is distorted by the reflected components summed with time delays proportional to the propagation delays of the reflection's path. (Image source: Amphenol)



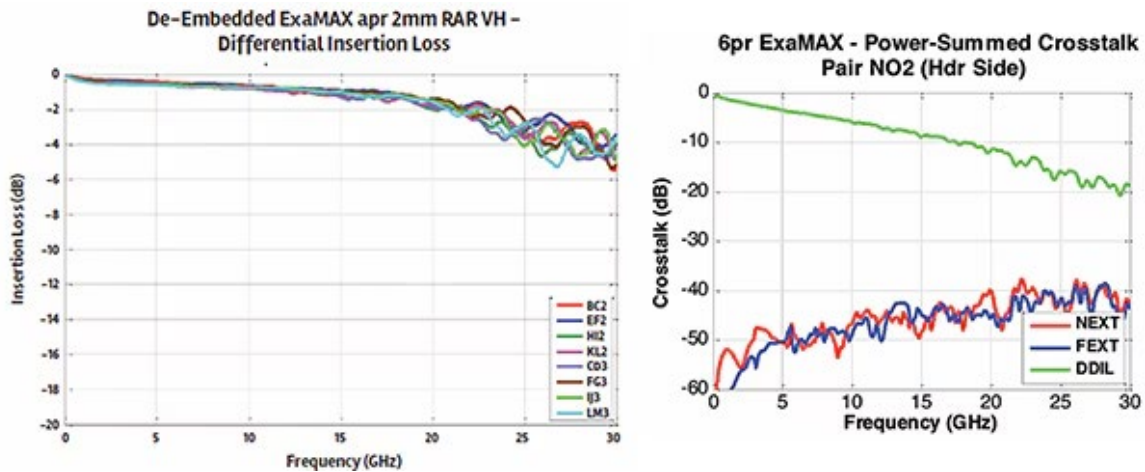


Figure 10: Shown are the significant insertion loss and crosstalk specifications as a function of frequency for the 10128419-101LF header. (Image source: Amphenol)

impedance and bandwidth. SI specifications include attenuation, velocity factor, return loss, insertion loss, and crosstalk.

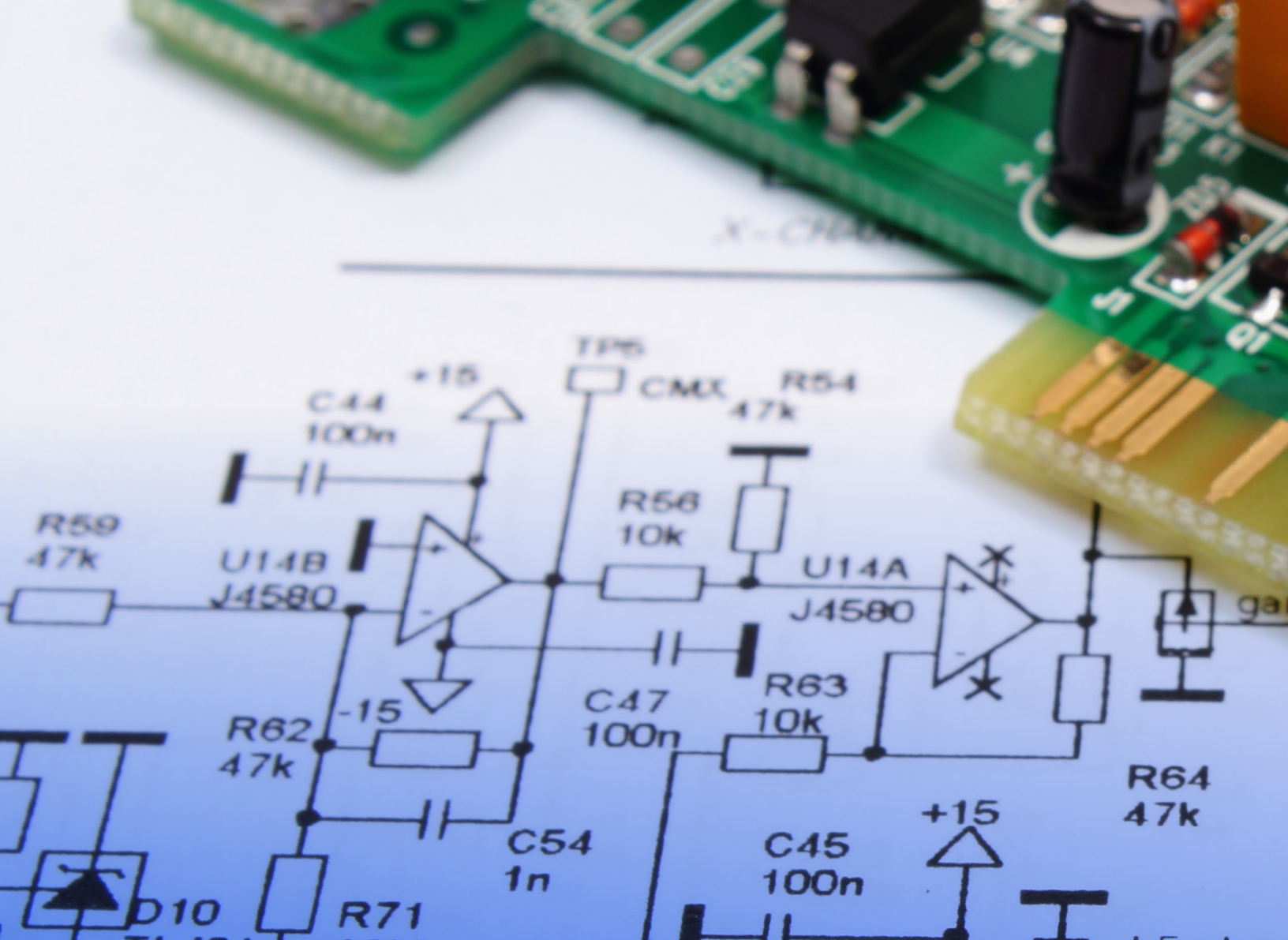
An example of a coaxial cable is [Times Microwave Systems' LMR-400-ULTRAFLEX](#) 50 Ω low-loss cable, rated for indoor or outdoor operation at 6 GHz. Its frequency-dependent attenuation is 0.05 dB/ft. at 900 megahertz (MHz) and increases to 0.13 dB/ft. at 5.8 GHz. Its propagation velocity, a specification used when dealing with reflections, is 80% of the speed of light (a velocity factor of 0.8). Reflection and transmission losses are length-dependent and are not given in bulk cable specifications.

Components such as connectors are specified somewhat differently. The [Amphenol Communications Solutions 10128419-101LF](#) 112-position male header connector is intended for backplane use. It is rated to handle digital signals with a maximum bit rate of 25 to 56 Gbps. Its contacts have a characteristic impedance of 92 Ω . As a multiconductor connector, its insertion loss and crosstalk specifications are critical (Figure 10).

These are typical SI specifications associated with interconnect components.

Conclusion

SI must be considered throughout the design process for high-speed systems such as AI data centers. Many factors can affect SI, and designers must account for them all to mitigate their effects. SI can be maximized with the proper PC board trace layout and appropriate conductors and connectors.



Accelerate your electronics projects with Scheme-it and DigiKey's extensive component catalog



The fastest way to design, source and build your next circuit online

Bringing an electronics project to life requires seamless circuit design tools, efficient component sourcing and smooth collaboration. Whether you're an electrical engineer, hobbyist, STEM educator or student, using the right resources eliminates friction and speeds up the process from concept to reality.

Scheme-it by DigiKey is a free, web-based schematic tool that simplifies circuit design. Integrated directly with DigiKey's vast catalog of over 15 million in-stock electronic components, including

many with graphic symbols, using Scheme-it ensures that your designs are not just creative but also immediately actionable. This article explores how Scheme-it evolved into a powerful design tool and how it streamlines the journey from circuit ideation to component selection and ordering.

From circuit ideation to component selection—all in one place

Switching between design software, supplier websites and inventory tools wastes valuable time. With Scheme-it, you can draw schematics, select available electronic components and create

a bill of materials (BOM) all within the same platform. The ability to choose from millions of in-stock components with built-in price and availability updates streamlines the process, making it easier to move from design to purchasing. DigiKey part numbers can be directly assigned, added to DigiKey's myLists or moved to your DigiKey cart, and ordered instantly.

The seamless transition from circuit design to development is supported through Scheme-it's KiCAD export feature, allowing you to take the next steps of the design journey into a complete EDA (Electronic Design Automation) tool without starting over. Its built-in sharing tools also allow users

to share their projects via URL or embedded within an electronic document, ensuring that design engineers can share their ideas easily and seamlessly. Users also have the option to print or export their project to PDF, PNG or SVG.

Speed up your design process with pre-built circuits

Starting from scratch can be time-consuming, which is why

Scheme-it includes a vast library of pre-built circuit designs and templates. Whether you're designing power supply circuits, amplifiers, IoT devices or industrial automation systems, Scheme-it provides ready-made circuit templates to accelerate the design process. Pre-designed AC/DC converter circuits, signal processing modules and sensor integration circuits make it easy to get started and to select compatible electronic components from DigiKey's catalog.

Schematics can be annotated using mathematics mark-up tools that support LaTeX and AsciiMath for adding equations (Figure 1).

Real-world example: ZigBee-based home automation circuit

One of reference designs in Scheme-it is a ZigBee-based home automation circuit using a 900 MHz wireless module. This

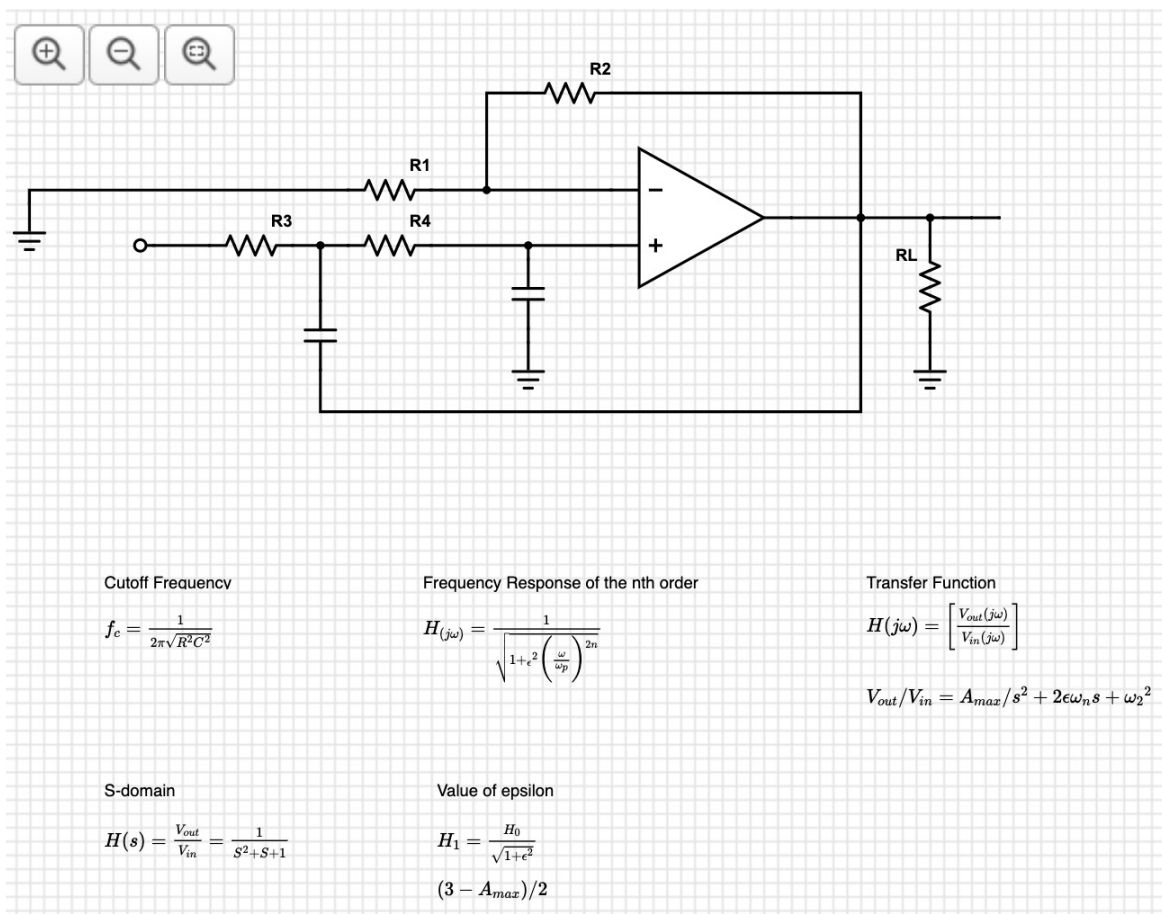


Figure 1:
This low-pass Butterworth circuit building block in Scheme-it includes design equations. (Image source: DigiKey)

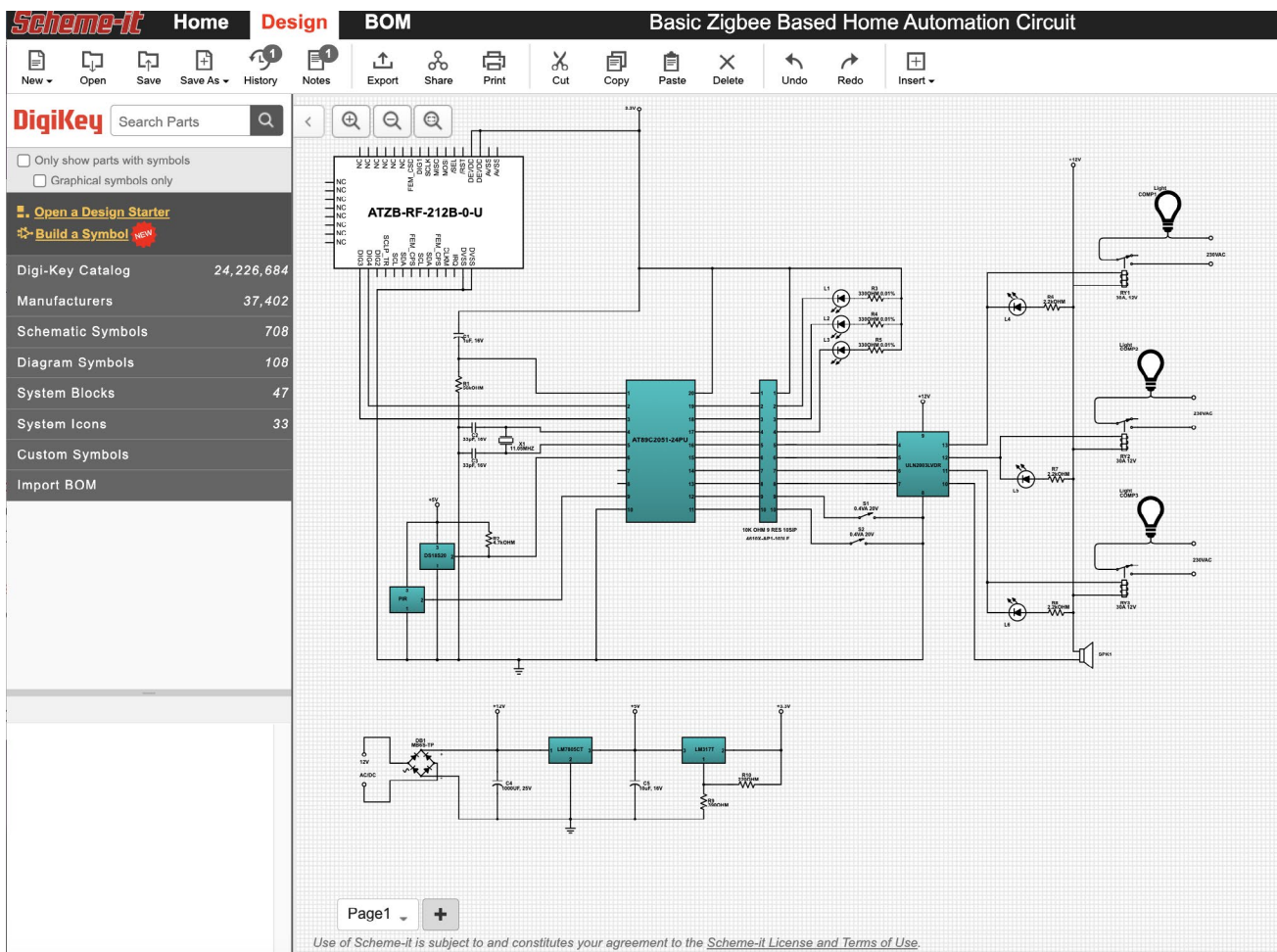


Figure 2: This basic ZigBee home automation circuit is one of the numerous ready-to-use designs included in Scheme-it. (Image source: DigiKey)

IoT project template includes components such as the AT89C2051-24PU microcontroller, DS18S20 temperature sensor and PIR motion detector.

Every component can be selected, added to a BOM and ordered directly from DigiKey – simplifying the entire prototyping process.

Who can benefit from Scheme-it and DigiKey?

Scheme-it and DigiKey provide an end-to-end solution that is perfect for engineers, hobbyists, educators and students, streamlining circuit design and component sourcing so you can focus on bringing your ideas to life. Professional engineers can

reduce design-to-prototype time by streamlining part selection and ordering. STEM educators and students can use Scheme-it for teaching electronics design, with access to real-world components for hands-on learning. Electronics hobbyists and makers can bring their ideas to life with user-friendly design tools and instant component availability.

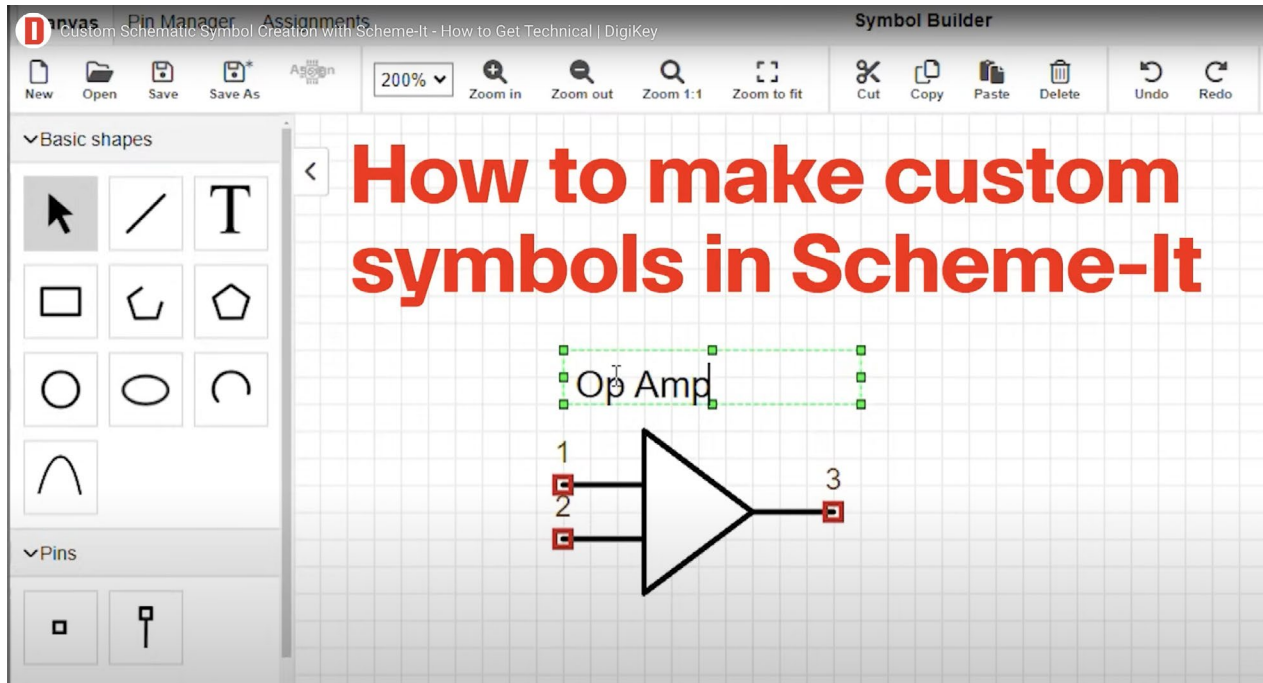


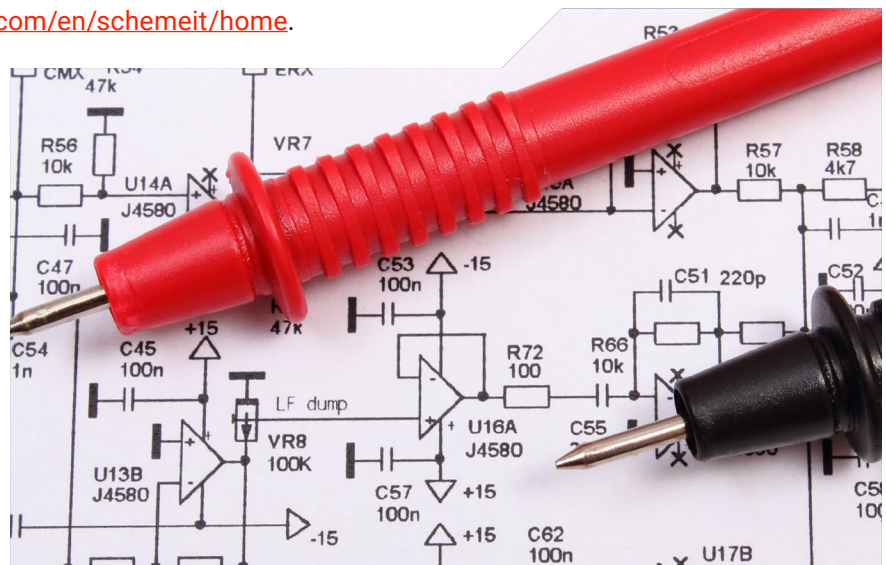
Figure 2: This basic ZigBee home automation circuit is one of the numerous ready-to-use designs included in Scheme-it. (Image source: DigiKey)

Turn your ideas into reality with Scheme-it and DigiKey

Designing and building circuits online has never been easier than using Scheme-it to create professional-grade diagrams and source the components you need – all in one place. Scheme-it is free to use, and its intuitive schematic editor enables users to create their circuit diagrams while ensuring they can source, purchase, and receive components without hassle. With millions of in-stock parts available for immediate purchase, DigiKey removes supply chain concerns and makes electronic design faster than ever.

Get started today! Design your next circuit with Scheme-it and instantly order components from DigiKey.

Try it now at <https://www.digikey.com/en/schemeit/home>.



Initial launch:

December 13, 2011:

- DigiKey introduced Scheme-it, an innovative, web-based schematic and diagramming tool designed to help engineers, educators, students, and hobbyists quickly design and share electronic circuits.

Key features at launch:

1. Browser-Based Interface:

Made accessible without requiring software installation.

2. Basic Component Library:

Included standard electrical and electronic symbols.

3. Diagramming Tools:

Allowed users to create simple circuit designs with drag-and-drop functionality.

4. Sharing Capability:

Provided basic export features like saving as PDFs or sharing via links.

Major milestones in Scheme-it's development:

2015–2016: Early Improvements

1. Enhanced Component Libraries:

Added more DigiKey catalog items to the tool.

2. Direct DigiKey Integration:

Linked components in schematics directly to DigiKey's product database for easy purchasing.

2020–2021: Significant Upgrades

■ October 2020: Launched Symbol Editor 2.0:

- Users could create custom symbols.
- Existing symbols became editable for better flexibility.

■ March 2021: Added Ultra Librarian Integration:

- Over 2 million component symbols from Ultra Librarian's extensive database were added.
- Users could search and integrate these symbols directly into their schematics.

■ Mathematics Markup: Supported LaTeX and AsciiMath for adding equations to schematics.

■ KiCad Export: Enabled users to export schematics into KiCad EDA software for PCB design.

These advancements solidified Scheme-it as a powerful, flexible tool for circuit design and prototyping.

The parts we sell help get you there safely



Today's cutting-edge vehicles can contain hundreds of sensors for systems that keep you comfortable, entertained, informed, and most importantly, safe.

The sensors we sell help engineers create these systems, but helping you enjoy your journey safely is what really drives us.

Find sensors for any application at [digikey.com](https://www.digikey.com)

DigiKey

we get technical

DigiKey is an authorized distributor for all supplier partners. New products added daily. DigiKey and DigiKey Electronics are registered trademarks of DigiKey Electronics in the U.S. and other countries. © 2025 DigiKey Electronics, 701 Brooks Ave. South, Thief River Falls, MN 56701, USA

 **ECIA MEMBER**
Supporting The Authorized Channel